Article

Cell Stem Cell

Cardiac Reprogramming Factors Synergistically Activate Genome-wide Cardiogenic Stage-Specific Enhancers

Graphical Abstract

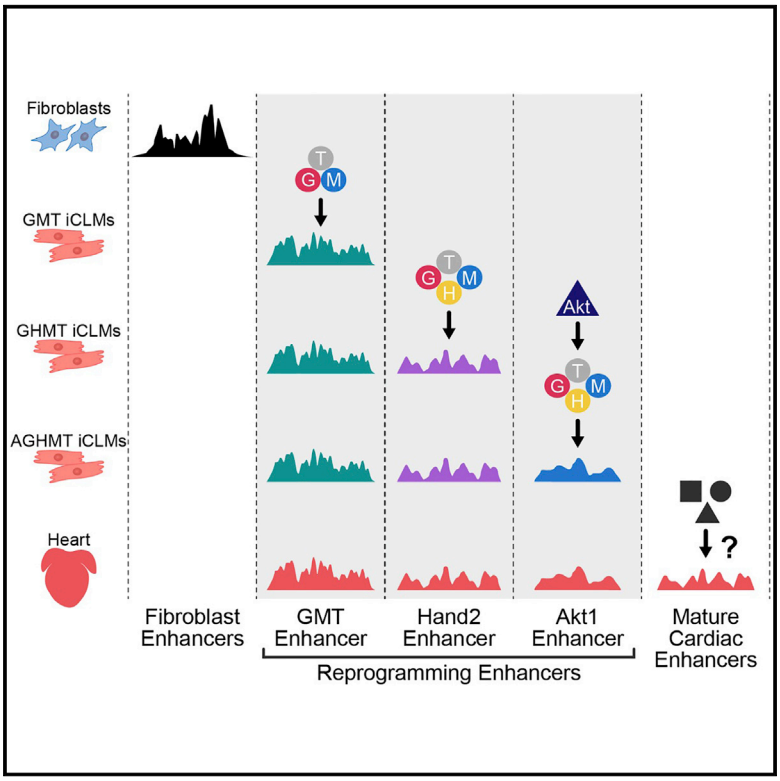

Authors

Hisayuki Hashimoto, Zhaoning Wang, Glynnis A. Garry, ..., Ning Liu, Rhonda Bassel-Duby, Eric N. Olson

Correspondence

eric.olson@utsouthwestern.edu

In Brief

Hashimoto and colleagues show that reprogramming factors act in concert at cardiac regulatory elements to directly reprogram mouse fibroblasts into induced cardiac-like myocytes (iCLMs). Moreover, cardiac reprogramming is achieved by activation of endogenous cardiac enhancers that initiate a cardiogenic gene regulatory network.

Highlights

- Reprogramming factors highly co-occupy regulatory elements during cardiac reprogramming
- Hand2 and Akt1 recruit reprogramming TFs to cardiac regulatory elements in iCLMs
- Cardiac reprogramming establishes an epigenetic landscape of heart development
- Inhibition of EGF receptor signaling augments cardiac reprogramming

Hashimoto et al., 2019, Cell Stem Cell *25*, 1–18
July 3, 2019
https://doi.org/10.1016/j.stem.2019.03.022

CellPress

Cell Stem Cell
Article

Cardiac Reprogramming Factors Synergistically Activate Genome-wide Cardiogenic Stage-Specific Enhancers

Hisayuki Hashimoto,[1] Zhaoning Wang,[1] Glynnis A. Garry,[1] Venkat S. Malladi,[2] Giovanni A. Botten,[1] Wenduo Ye,[1] Huanyu Zhou,[1] Marco Osterwalder,[3] Diane E. Dickel,[3] Axel Visel,[3,4,5] Ning Liu,[1] Rhonda Bassel-Duby,[1] and Eric N. Olson[1,6,*]

[1]Department of Molecular Biology, the Hamon Center for Regenerative Science and Medicine, and Senator Paul D. Wellstone Muscular Dystrophy Cooperative Research Center, University of Texas Southwestern Medical Center, 5323 Harry Hines Boulevard, Dallas, TX 75390, USA

[2]Department of Bioinformatics, University of Texas Southwestern Medical Center, 5323 Harry Hines Boulevard, Dallas, TX 75390, USA

[3]Environmental Genomics and Systems Biology Division, Lawrence Berkeley National Laboratory, 1 Cyclotron Road, Berkeley, CA 94720, USA

[4]US Department of Energy Joint Genome Institute, Walnut Creek, CA 94598, USA

[5]School of Natural Sciences, University of California, Merced, Merced, CA 95343, USA

[6]Lead Contact

*Correspondence: eric.olson@utsouthwestern.edu

https://doi.org/10.1016/j.stem.2019.03.022

SUMMARY

The cardiogenic transcription factors (TFs) Mef2c, Gata4, and Tbx5 can directly reprogram fibroblasts to induced cardiac-like myocytes (iCLMs), presenting a potential source of cells for cardiac repair. While activity of these TFs is enhanced by Hand2 and Akt1, their genomic targets and interactions during reprogramming are not well studied. We performed genome-wide analyses of cardiogenic TF binding and enhancer profiling during cardiac reprogramming. We found that these TFs synergistically activate enhancers highlighted by Mef2c binding sites and that Hand2 and Akt1 coordinately recruit other TFs to enhancer elements. Intriguingly, these enhancer landscapes collectively resemble patterns of enhancer activation during embryonic cardiogenesis. We further constructed a cardiac reprogramming gene regulatory network and found repression of EGFR signaling pathway genes. Consistently, chemical inhibition of EGFR signaling augmented reprogramming. Thus, by defining epigenetic landscapes these findings reveal synergistic transcriptional activation across a broad landscape of cardiac enhancers and key signaling pathways that govern iCLM reprogramming.

INTRODUCTION

Ischemic heart disease, caused by myocardial infarction, is the leading cause of death worldwide (Roth et al., 2017). After myocardial infarction, cardiomyocytes (CMs) are lost and replaced by a fibrotic scar, due to the minimal regenerative capacity of the adult heart. The damaged heart subsequently undergoes a pathological remodeling process, leading to cardiac dysfunction and heart failure with poor prognosis (Cohn et al., 2000). Current heart failure therapies are based on drugs or electromechanical devices. There is a major unmet need for alternative therapies to treat ischemic heart disease (Hashimoto et al., 2018).

To potentially overcome these issues, we and others have tested an alternative approach to directly reprogram resident cardiac fibroblasts (CFs) into induced cardiac-like myocytes (iCLMs) by cardiogenic transcription factors (TFs), bypassing the pluripotent state. Direct cardiac reprogramming was first achieved by forced expression of Gata4, Mef2c, and Tbx5 (referred to as GMT) in fibroblasts (Ieda et al., 2010). However, the reprogramming efficiency by GMT was relatively low. Addition of other factors to the GMT cocktail improves reprogramming efficiency, including Hand2 (referred to as GHMT) and a constitutively active form of Akt1 to GHMT (referred to as AGHMT) (Abad et al., 2017; Addis et al., 2013; Mohamed et al., 2017; Muraoka et al., 2014; Song et al., 2012; Yamakawa et al., 2015; Zhao et al., 2015; Zhou et al., 2015, 2017). Alternative approaches using different TF cocktails or combinations of microRNAs (miRNAs) and chemicals have also been shown to achieve and enhance cardiac reprogramming (Fu et al., 2015; Jayawardena et al., 2012; Lalit et al., 2016; Wang et al., 2014).

It is well known that many TFs act through combinatorial interactions to govern organ development and cell-type-specific differentiation (Spitz and Furlong, 2012). In this regard, the cardiac reprogramming factors Gata4, Mef2c, Tbx5, and Hand2 are key regulators of heart development, but their expression and biological functions are not limited to the heart (Galdos et al., 2017; Harvey, 2002; Olson, 2006). Additionally, although genome-wide transcriptome profiling has demonstrated the upregulation of cardiac markers and downregulation of fibroblast markers during cardiac reprogramming (Zhou et al., 2015), the mechanism by which these factors orchestrate reprogramming remains unclear.

We sought to study the molecular mechanisms by which cardiac reprogramming factors contribute to cell-fate conversion

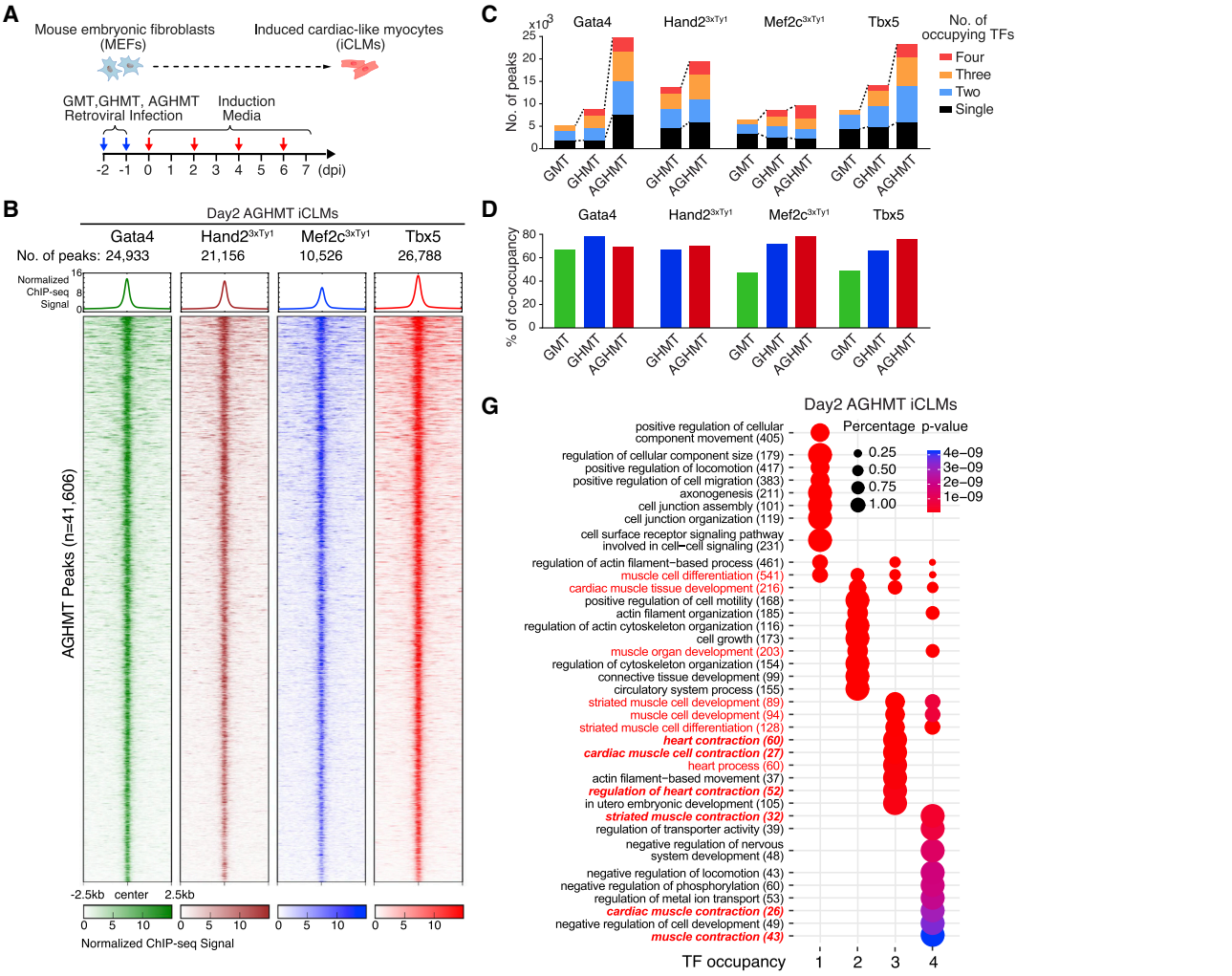

(legend on next page)

using a genome-wide approach. Here, we used chromatin immunoprecipitation followed by massively parallel DNA sequencing (chromatin immunoprecipitation sequencing [ChIP-seq]) to profile the genomic binding sites of reprogramming TFs and the landscape of active enhancers, annotated by H3K27ac histone modification, during cardiac reprogramming (Creyghton et al., 2010). We found that reprogramming TFs rapidly silence fibroblast enhancers and synergistically activate cardiac enhancers predominantly enriched with Mef2 motifs. Addition of Hand2 and Akt1 to GMT expands TF co-occupancy and activates additional cardiac enhancers, which further augments cardiac gene expression. Moreover, additional cardiac enhancers were sequentially activated during the reprogramming process, in accordance with the temporal acquisition of functional phenotypes in iCLMs. We discovered that subsets of conserved reprogramming enhancers displayed unique spatial expression patterns in the developing heart. Finally, by constructing a gene regulatory network (GRN) from our genomic data, we found that EGF receptor signaling is directly suppressed by reprogramming TFs and that inhibition of EGF and Jak2 signaling augmented reprogramming in fibroblasts. Our study describes the epigenomic dynamics that underlie cardiac reprogramming, which is cooperatively orchestrated by reprogramming factors to convert fibroblasts toward a cardiac lineage.

RESULTS

Rapid Genome-wide Co-occupancy of Reprogramming Factors during Reprogramming

To gain insights into the molecular mechanisms of fibroblast to CM reprogramming, we initially examined the recruitment of reprogramming factors to genomic DNA binding sites using ChIP-seq. To determine the timing of the reprogramming process, we first quantified the expression of the cardiac markers, Tnnt2 and Myh6, in mouse embryonic fibroblasts (MEFs) reprogrammed by retroviral expression of GMT, GHMT, and AGHMT, after 2 and 7 days of reprogramming (Figures 1A and S1A). Expression of both cardiac markers was detectable as early as day 2 (Figure S1A). Therefore, we sought to identify genomic binding sites for Gata4, Hand2, Mef2c, and Tbx5 in MEFs 2 days after reprogramming by the AGHMT cocktail. Hand2 and Mef2c were tagged with 3xTy1 since currently available antibodies for Hand2 and Mef2c are inadequate for ChIP. We confirmed that the 3xTy1 tag did not affect the expression or reprogramming efficiency of these TFs by western blotting, immunostaining, Ca^{2+} flux, and beating (Figures S1B–S1F). ChIP-seq analysis performed on day 2 AGHMT iCLMs revealed that reprogramming TFs rapidly occupy chromatin sites, and we identified 24,933 total peaks (binding sites) for Gata4, 21,156 for Hand2, 10,526 for Mef2c, and 26,788 for Tbx5 (Figure 1B).

To assess the distribution of genomic binding sites occupied by the TFs in response to the AGHMT cocktail, we plotted the ChIP signals that were present in at least one of the peaks for Gata4, Hand2, Mef2c, and Tbx5 (defined as AGHMT peaks; total n = 41,606). Interestingly, this analysis revealed substantial co-occupancy of reprogramming TFs, with ~50% of peaks being co-occupied by at least two TFs at these regions (Figure 1B; Table S1). These findings suggest that Gata4, Hand2, Mef2c, and Tbx5 are synchronously recruited to genomic sites during cardiac reprogramming. To understand the effect of Hand2 and Akt1 on TF binding, we repeated ChIP-seq in day 2 GMT and GHMT iCLMs and similarly found co-occupancy of TFs in genomic binding sites during GMT and GHMT reprogramming, albeit to reduced proportions compared to AGHMT (~33% and ~46% of peaks were co-occupied, respectively) (Figures S2A and S2B; Table S1).

Since the percentage of co-occupancy differed between reprogramming cocktails, we analyzed the occurrence of co-occupancy among individual TF peaks (Table S1). Interestingly, addition of Hand2 increased the proportion of co-occupancy in Gata4, Mef2c, and Tbx5 peaks, indicating the recruitment of these TFs to additional chromatin sites by Hand2 (Figures 1C and 1D). To further define the Hand2-responsive elements, we performed *de novo* motif discovery of the Hand2 peaks using HOMER (Heinz et al., 2010). Consistently, motifs recovered from Hand2 peaks matched the consensus E-box motif, a DNA element that is usually bound by basic helix-loop-helix (bHLH) proteins, such as Hand2 (Figure 1E) (Laurent et al., 2017). Moreover, Hand2 peaks were enriched for consensus motifs for Gata4, Mef2c, and Tbx5, suggesting that these factors may directly bind to Hand2-enriched binding sites. Other enriched motifs corresponded to consensus sites for binding of TF AP-1 and TEA domain family member 1 (Tead1), which are known transcriptional regulators of heart development (Jahangiri et al., 2016; Yoshida, 2008).

Addition of Akt1 dramatically increased the number of Gata4 binding sites, consistent with previous reports demonstrating Gata4 transcriptional regulation by the Akt1/GSK3 β pathway (Condorelli et al., 2002; Morisco et al., 2001) (Figure 1C). Since

Figure 1. Genome-wide Co-occupancy of Reprogramming Factors in AGHMT iCLMs

(A) Strategy for cardiac reprogramming in MEFs. (dpi, days post-induction.)

(B) ChIP-seq data for Gata4, Hand2, Mef2c, and Tbx5 display co-occupancy at 41,606 genomic binding sites in day 2 AGHMT iCLMs. ChIP-seq signal heatmap using a 5 kb window was centered on peak regions and sorted in descending order by signal intensity.

(C) Number of TF peaks of GMT, GHMT, and AGHMT in day 2 iCLMs.

(D) Percentage of TF peaks co-occupied by more than two TFs.

(E) *De novo* motifs identified at Hand2 bound sites in day 2 iCLMs by HOMER.

(F) Number of TF peaks with different pairs of TFs in day 2 iCLMs.

(G) TF peaks were annotated to the nearest neighboring genes, and GO enrichment analysis was performed with DAVID (v.6.8). GO enrichment from different groups based on the number of occupying TFs was performed with clusterProfiler (v.3.6.0).

(H) Genome browser view showing the co-occupancy of Gata4, Hand2, Mef2c, and Tbx5 in a 70 kb window encompassing *Tnni1*, *Lad1*, and *Tnnt2* genes in day 2 iCLMs.

(I) GMT, GHMT, and AGHMT ChIP-seq peaks were classified into seven genomic categories. Dashed lines connect the group of intronic and intergenic TF peaks. See also Figures S1 and S2 and Table S1.

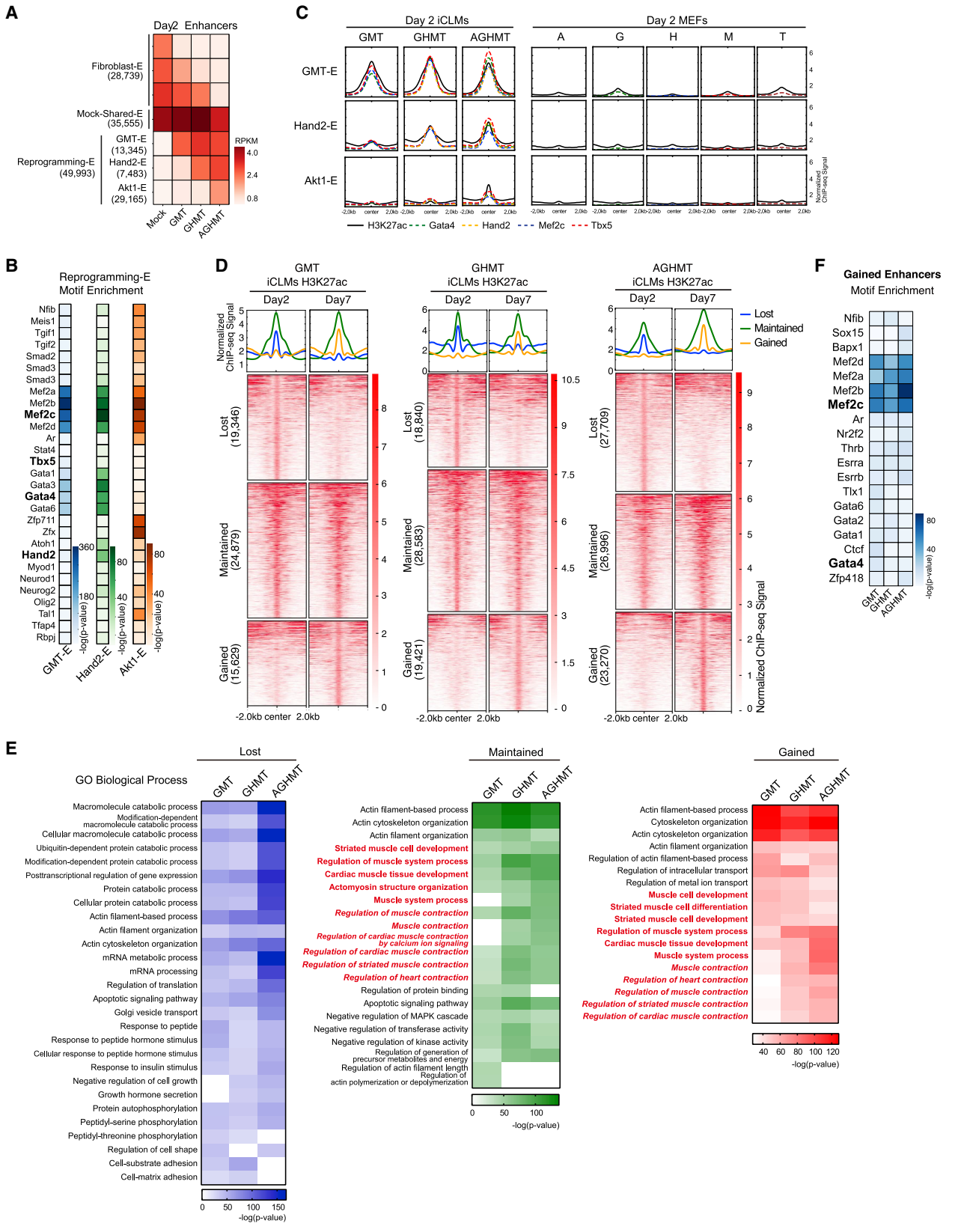

(legend on next page)

Gata4 is known to physically interact with Mef2c, Hand2, and Tbx5 and thereby synergistically activate cardiac gene expression, we analyzed the number of TF peaks shared by different pairs of reprogramming TFs (Ang et al., 2016; Dai et al., 2002; Maitra et al., 2009; Morin et al., 2000). Akt1 significantly expanded the co-binding sites of Gata4-Hand2 (GH) and Gata4-Tbx5 (GT) pairs, suggesting Gata4 is a key factor in enhancement of reprogramming by Akt1 (Figure 1F). Although these binding pairs increased with the addition of Hand2, the increase was not as striking in comparison to Akt1. Thus, Hand2 expanded the co-occupancy of reprogramming TFs, whereas Akt1 increased the total number of binding sites.

To gain broader insights into the significance of TF co-occupancy, we annotated each TF peak to its nearest neighboring gene and compared gene ontology (GO) term enrichment among the TF peaks clustered by the number of TFs bound using clusterProfiler (Yu et al., 2012). Remarkably, annotation of co-occupied TF binding sites compared to single TF peaks in GMT (Figure S2C), GHMT (Figure S2D), and AGHMT (Figure 1G) showed stronger enrichment in heart- or muscle-related GO terms, with higher significance in GHMT and AGHMT iCLMs. As a representative example, the promoter region of *Tnnt2*, which encodes cardiac muscle troponin T, displayed co-occupancy of Gata4, Hand2, Mef2c, and Tbx5 in day 2 AGHMT iCLMs (Figure 1H).

Since addition of Hand2 and Akt1 increased the number of TF peaks, we analyzed the location of these TF peaks to see whether there were any commonalities among the newly generated peaks. Interestingly, we found that addition of Hand2 and Akt1 decreased the proportion of TF peaks in promoter regions and increased binding at introns and intergenic regions (Figures 1I and S2E). This pattern suggests that Hand2 and Akt1 may function to coordinate the recruitment of TFs to potential enhancer elements.

Reprogramming Factors Coordinate the Activation of Cardiac Enhancers

Although activation at gene promoters is important for transcriptional regulation, distal enhancers play a pivotal role in directing tissue-specific gene expression, especially during lineage commitment in development (Creyghton et al., 2010; Wamstad et al., 2012). The activation of a distinct enhancer network may underlie direct cardiac reprogramming, and we sought to characterize this regulatory landscape by performing ChIP-seq for the active enhancer histone mark, H3K27ac, after 2 days of cardiac reprogramming (Creyghton et al., 2010). We recovered between 80,000 and 100,000 H3K27ac peaks in mock-infected MEFs and iCLMs reprogrammed with GMT, GHMT and AGHMT. Of these, peaks that were present in promoter regions (−2,000 to +2,000 bp from the transcription start site [TSS]) were excluded from further analyses to focus on cardiac enhancers (King et al., 2016). We then compared the H3K27ac enhancer peaks among different populations in day 2 iCLMs and clustered them into three groups: H3K27ac peaks in fibroblasts that were lost in iCLMs (Fibroblast-E), maintained during the cardiac reprogramming process (Mock-Shared-E), and enriched specifically in iCLMs (Reprogramming-E) (Figure 2A). Among the Fibroblast-E peaks, we identified subsets of enhancers that were silenced in response to GMT, Hand2 (GHMT), or Akt1 (AGHMT) (Figure 2A).

To identify enhancers uniquely activated by Hand2 and Akt1, we then focused on those histone marks present only during the cardiac reprogramming process (Reprogramming-E) and compared these among the different iCLM populations. We were able to cluster the Reprogramming-E peaks into the following groups: H3K27ac enhancer peaks that were maintained among GMT, GHMT, and AGHMT reprogramming (GMT-E, n = 13,345), responsive to Hand2 (Hand2-E, n = 7,483), and responsive to Akt1 (Akt1-E, n = 29,165) (Figures 2A and S3A). To evaluate the functional relevance of these subgroups of enhancer regions, we annotated the peaks to nearest genes using Genomic Regions Enrichment of Annotations Tool (GREAT) (McLean et al., 2010). This *in silico* analysis revealed that genes associated with the GMT-E and Hand2-E peaks associated strongly with the GO term for muscle system process (Figure S3B). Additionally, these genes showed expression patterns detected in the cardiovascular system based on the Mouse Genomics Informatics (MGI) database. In contrast, annotation of Akt1-E peaks did not show strong enrichment in muscle- or heart-related GO terms but rather strong enrichment related to chromatin and histone modification (Figure S3B). This may suggest that Akt1 acts indirectly to further activate regulatory elements during the reprogramming process.

To define the relationship between enhancers and reprogramming TF binding, we performed a motif discovery of the Reprogramming-E peaks using HOMER. Indeed, all four reprogramming TF consensus motifs were enriched in the Reprogramming-E peaks. However, Mef2c motifs were most dominantly represented in all three of the Reprogramming-E groups, suggesting that transcriptional activation is mainly occurring in the vicinity of Mef2c binding sites (Figure 2B; Table S2). We then overlapped these enhancer regions with the reprogramming TF binding sites

Figure 2. Synergistic Enhancer Activation during Reprogramming

(A) H3K27ac enhancer peaks in day 2 iCLMs clustered into three groups (Fibroblast-Enhancer, Mock-Shared-Enhancer, and Reprogramming-Enhancer). Fibroblast-Enhancer and Reprogramming-Enhancer were then sub-clustered into groups depending on their response to GMT, GHMT, and AGHMT (GMT-E, Hand2-E, and Akt1-E for Reprogramming-E). Each box represents the mean RPKM H3K27ac enhancer signals of the group of enhancers.

(B) Heatmaps of known motifs enriched in GMT-E, Hand2-E, and Akt1-E peaks.

(C) Normalized ChIP-seq binding profiles for H3K27ac and TFs show similar distribution patterns on a genome-wide scale in iCLMs. TF peaks show higher correlation with Hand2-E and Akt1-E peaks in the presence of Hand2 and Akt1, respectively. Single-factor overexpressing MEFs show weak signals of H3K27ac and TF binding at the Reprogramming-E regions.

(D) Heatmaps of reprogramming enhancers clustered into three distinct groups depending on differences between day 2 and 7 iCLMs.

(E) Heatmaps of overrepresented terms belonging to the Biological Process GO in each enhancer cluster. Terms related to heart or muscle contraction are highlighted in red italics.

(F) Heatmap of known motifs enriched in enhancers gained by day 7 compared to day 2 iCLMs.

See also Figure S3 and Tables S2 and S3.

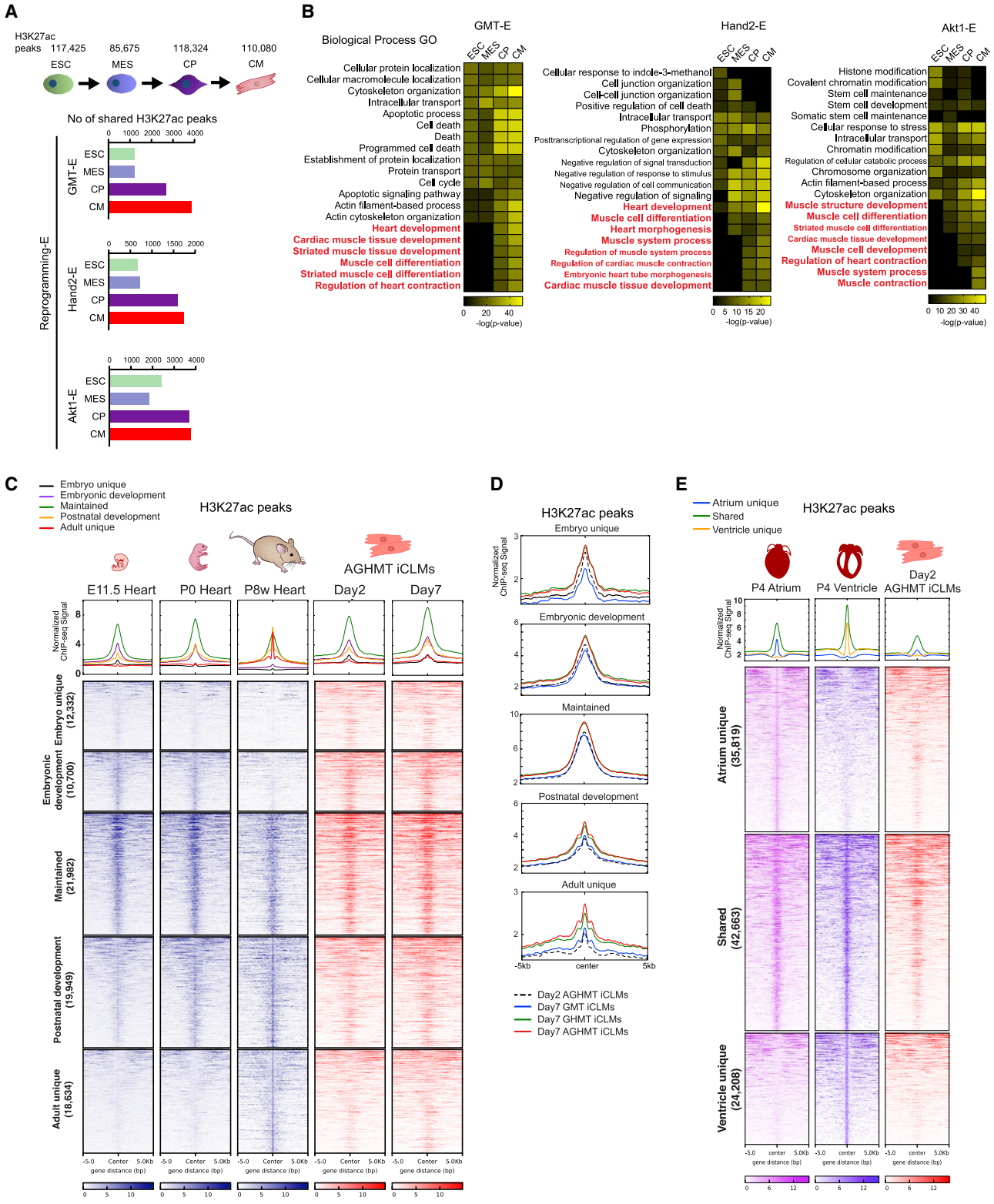

Figure 3. Conservation of the Reprogramming Enhancer Landscape in Cardiogenic Processes

(A) Comparison of Reprogramming-E peaks with active enhancers in embryonic stem cells (ESC), mesoderm (MES), cardiac precursors (CP), and cardiomyocytes (CM).

(legend continued on next page)

previously identified (Figures 1B, S2A, and S2B). Accordingly, the Reprogramming-E regions showed an abundant overlap with multiple reprogramming TF binding sites (Figure 2C). Interestingly, although Hand2-E and Akt1-E peaks were enriched with reprogramming TF motifs, TF binding at these regions was dependent on Hand2 and Akt1, respectively (Figure 2C). This indicates that Hand2 and Akt1 facilitate TF access to these enhancer regions enriched with Mef2c motifs, thereby increasing the co-occupancy of reprogramming TFs.

To determine whether a single reprogramming factor can sufficiently activate reprogramming enhancers, we also performed H3K27ac and TF ChIP-seq in MEFs solely overexpressing each single factor, 2 days post-infection. Each single factor showed approximately 25,000–45,000 newly generated H3K27ac peaks compared to mock-infected cells (Figure S3C). Although these single-factor unique enhancers (SFEs) (Akt1-SFE, Gata4-SFE, Hand2-SFE, Mef2c-SFE, and Tbx5-SFE) showed some overlap in their peaks, known motif discovery revealed that SFE regions were not highly enriched with all four reprogramming TF motifs (Figures S3D and S3E). Additionally, GO analysis of the single-factor responsive enhancers did not show enrichment with heart- or muscle-related terms (Figure S3F). Most importantly, single-factor responsive enhancers and single-factor TF peaks did not show strong signals in the Reprogramming-E regions (Figure 2C). Together, these data suggest that the initial process of cardiac reprogramming is activated by cooperative actions of cardiogenic factors at regulatory elements highly enriched with Mef2c binding sites.

To further explore the temporal dynamics of the reprogramming enhancers, we performed H3K27ac ChIP-seq in day 7 iCLMs and compared the enhancer profile with day 2 iCLMs, since spontaneous beating initiates around day 7 in AGHMT-induced iCLMs. We then clustered day 2 and day 7 iCLM enhancers into three distinct groups: those enhancer sites that were lost, maintained, or gained by day 7 relative to day 2 iCLMs (Figure 2D). Enhancers lost by day 7 displayed GO terms related to general cellular processes such as catabolic and mRNA processes, transcriptional regulation, and protein phosphorylation (Figure 2E). In contrast, annotation of the enhancers gained or maintained by day 7 revealed a significant association with GO terms related to cytoskeleton processes and heart or muscle processes including differentiation, development, and contraction (Figure 2E). This suggests that, after the activation of the reprogramming enhancer landscape on day 2, additional time is required for establishment of the mature cardiac enhancer landscape. Interestingly, motif discovery at enhancers gained by day 7 in all three iCLM groups again yielded strong enrichment of Mef2c consensus motifs, indicating a persistent regulatory function of Mef2c for maturation during reprogramming (Figure 2F; Table S3). However, gained enhancers in GMT, GHMT, and AGHMT were mostly unique to each cocktail (Figure S3G). The strong enrichment of heart- and muscle-related GO terms in gained enhancers of GHMT and AGHMT-treated iCLMs suggests that Hand2 and Akt1 also carry out a unique role in iCLM maturation. The distinct effect of Hand2 and Akt1 in enhancing iCLM maturation is also supported by the fact that day 2 Hand2-E and Akt1-E regions are not sufficiently activated later in day 7 mock or GMT iCLMs (Figure S3H).

Cardiac Reprogramming Shares Enhancers with Cardiogenic Processes

To explore the relationship between cardiac enhancer activation during reprogramming and other cardiogenic processes, we first compared reprogramming enhancers with enhancers activated during cellular differentiation. By using an embryonic stem cell (ESC) cardiac differentiation H3K27ac ChIP-seq dataset, we first overlapped Reprogramming-E regions from Figure 2A with the active enhancers in different stages defined as ESC, mesoderm (MES), cardiac precursor (CP), and CM by stage-specific expression of functionally related genes (Wamstad et al., 2012). Interestingly, Reprogramming-E regions showed overlap with all four differentiation stages but predominantly with CP and CM stages (Figure 3A). GO analysis of these overlapping enhancers using GREAT showed enrichment of terms related to heart or muscle differentiation, development, and contraction, particularly in CP and CM stages (Figure 3B). These findings suggest that the direct cardiac reprogramming process follows an epigenetic trajectory of cellular differentiation primarily from the CP stage.

We then compared the enhancer landscape of AGHMT-treated iCLMs with ENCODE H3K27ac datasets of hearts from different developmental stages to reveal the relationship between reprogramming and heart development (Consortium, 2012). We first clustered active heart enhancers according to their appearance in different developmental stages: active enhancers that are unique to E11.5 heart (Embryo unique), shared among E11.5 and P0 hearts (Embryonic development), shared among E11.5, P0, and P8 week hearts (Maintained), shared among P0 and P8 week hearts (Postnatal development), and unique to P8 week heart (Adult unique) (Figure 3C). Strikingly, AGHMT iCLM enhancer peaks showed the strongest signal intensity in the Maintained cluster regions, then in the Embryonic development and Postnatal development cluster regions, and weak signal intensity in the Embryo unique and Adult unique cluster regions (Figure 3C). This explains that, among these three developmental stages, iCLMs represent a similar enhancer landscape to that of the neonatal heart, where the heart is switching from embryonic to adult enhancers. Interestingly, day 7 AGHMT iCLM enhancers showed stronger enrichment in Postnatal development and Adult unique clusters compared to day 2 AGHMT iCLMs (Figure 3D). Moreover, day 7 AGHMT iCLM enhancers also showed stronger enrichment in these two clusters compared to day 7 GMT and GHMT iCLM enhancers (Figure 3D).

(B) Heatmaps of overrepresented terms belonging to the Biological Process GO using GREAT in each reprogramming enhancer cluster.

(C) Heatmaps of H3K27ac enhancer ChIP-seq signals of E11.5, P0, and P8 week hearts from ENCODE datasets, and day 2 and 7 AGHMT iCLMs clustered according to their appearance in different developmental stages.

(D) Normalized ChIP-seq binding profiles for H3K27ac of day 2 AGHMT, and day 7 GMT, GHMT, and AGHMT iCLMs, in each developmental cluster from Figure 3C are shown.

(E) Heatmap of H3K27ac enhancer ChIP-seq signals of P4 atrium, ventricle, and day 2 AGHMT iCLMs using a 10 kb window, clustered according to their presence in P4 atrium and ventricle. Normalized ChIP-seq binding profiles for H3K27ac in each cluster are shown.

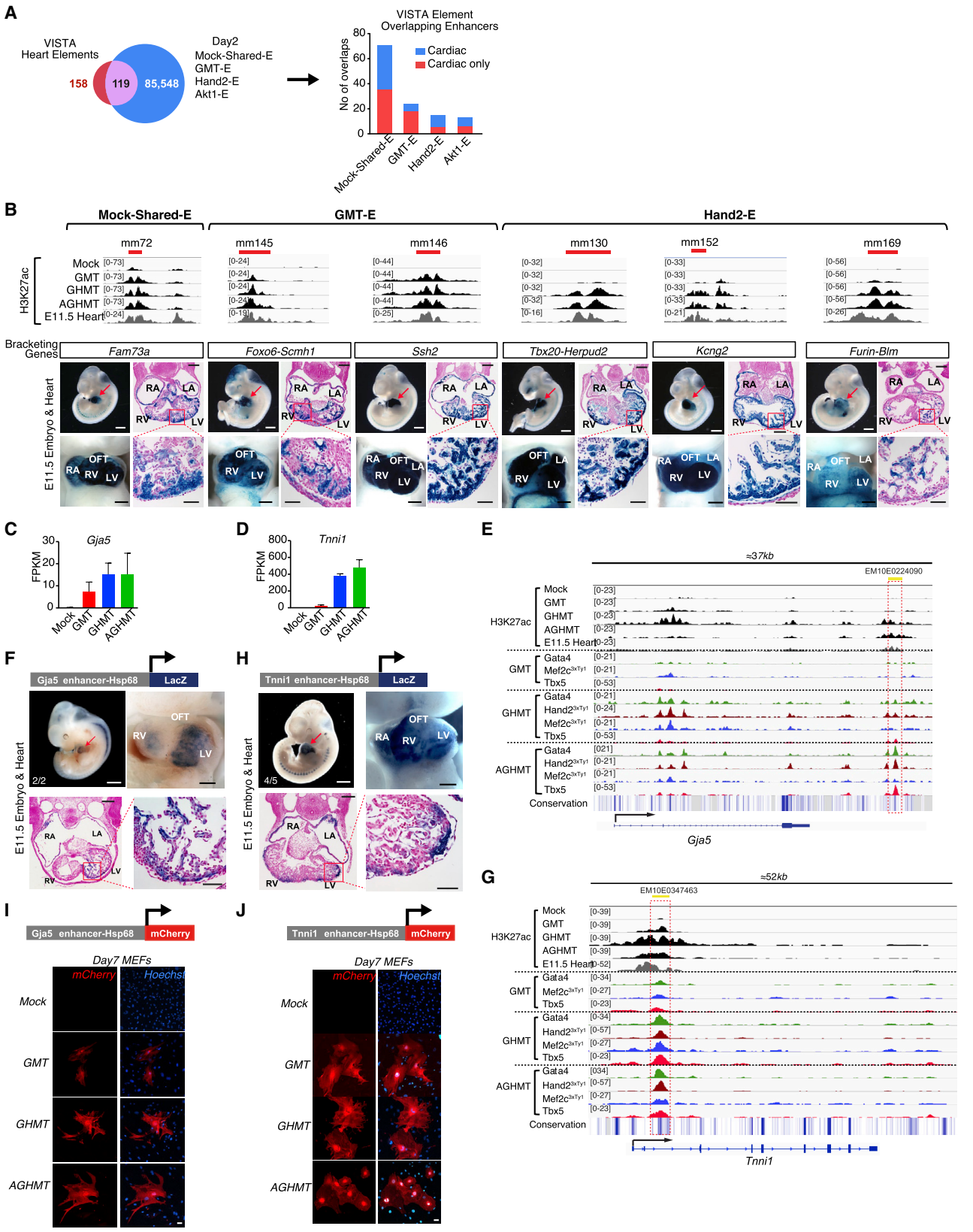

(legend on next page)

These findings suggest that continuous culture of iCLMs and addition of Hand2 and Akt1 both enable iCLMs to gain active enhancers unique to the postnatal heart as it matures (Figure 3D).

We were also interested in whether iCLM enhancers show any correlation with sub-regional cardiac enhancers *in vivo*. To define these enhancers, we performed H3K27ac ChIP-seq on P4 atrium and ventricle, since the neonatal heart demonstrates the highest similarity with iCLM enhancers. We then clustered enhancers active in P4 atrium and ventricle using a similar approach as in our previous analyses: active enhancers that are unique to P4 atrium (Atrium unique), shared among P4 atrium and ventricle (Shared), and unique to P4 ventricle (Ventricle unique) (Figure 3E). Overlap with the day 2 AGHMT iCLM enhancers showed that iCLMs are predominantly enriched with "Shared" enhancers, consistent with our previous report of diverse cardiac cell types induced during cardiac reprogramming (Nam et al., 2014).

Overall, these analyses revealed commonalities in enhancer activation between cardiac reprogramming and other cardiogenic processes. Although iCLMs are epigenetically linked to CP and CM stages in terms of lineage commitment, iCLMs are still immature, demonstrating closest similarity to neonatal heart enhancers and lacking activation of maturation enhancers.

Reprogramming Enhancers Display Diverse Cardiac Expression Patterns *In Vivo*

To determine whether reprogramming enhancers were also active *in vivo*, we overlapped iCLM enhancers (Mock-Shared-E and Reprogramming-E) with enhancers shown to be active in the mouse heart as verified in the VISTA Enhancer Browser (Blow et al., 2010; Visel et al., 2007). Of our iCLM enhancers, 119 enhancers overlapped with 158 mouse heart enhancers available in the VISTA dataset, confirming the *in vivo* cardiac activity of certain reprogramming enhancers (Figure 4A; Table S4). Analysis of transgenic mouse LacZ enhancer reporter assays on 18 elements from the 119 overlapping VISTA elements revealed the subregional cardiac activity of iCLM enhancers, which showed strong LacZ signal localized in the myocardium of the embryonic heart at E11.5 (Figures 4B, S4A, and S4B; Table S5). This finding that reprogramming enhancers display various subregional *in vivo* cardiac activity patterns is compatible with our previous analysis showing strongest enrichment of reprogramming enhancer signals in atrium and ventricle shared enhancer regions (Figure 3E).

We also tested two reprogramming enhancers that did not overlap with the mouse VISTA heart elements using transgenic mouse reporter assays. We chose two enhancers co-occupied by TFs that neighbor the genes *Gja5* or *Tnni1*, since these two genes are well characterized and strongly upregulated during reprogramming (Figures 4C and 4D). *Gja5* encodes Connexin 40 (Cx40), a gap junction protein that plays an important role in the cardiac conduction system (Bagwe et al., 2005). We identified a highly conserved enhancer ~25 kb downstream of *Gja5*, which was activated and associated with TF co-occupancy during cardiac reprogramming in the presence of Hand2 (Figure 4E). This 664 bp enhancer is a short fragment homologous to part of the VISTA human element hs2126 (5,192 bp) and also partially overlapped with a candidate regulatory element EM10E0224090 from Search Candidate Regulatory Elements by ENCODE (SCREEN) (Consortium, 2012; Dickel et al., 2016). LacZ staining confirmed strong activity of this putative *Gja5* enhancer (Gja5-E) in the myocardium of multiple chambers at E11.5 as well as at other stages of embryonic development (Figures 4F and S5A). *Tnni1* encodes the predominant Troponin I isoform expressed in embryonic skeletal and cardiac muscle (Corin et al., 1994). We identified a highly conserved enhancer (1,171 bp) in an intronic region of *Tnni1*, which was activated and associated with TF co-occupancy during reprogramming, and partially overlapped with SCREEN candidate regulatory element EM10E0347463 (Figure 4G). LacZ staining confirmed strong activity of this

Figure 4. *In Vivo* Cardiac Activity of Reprogramming Enhancers

(A) iCLM enhancers (Mock-Shared-E + GMT-E + Hand2-E + Akt1-E from Figure 2A) were overlapped with 158 mouse heart enhancers from the VISTA enhancer database, which showed an overlap of 119 enhancers. Numbers of iCLM enhancers in different groups overlapping with the VISTA heart enhancers are shown. "Cardiac only" indicates enhancers that show exclusively cardiac activity and "Cardiac" indicates enhancers that show activity in the heart plus other tissues, based on the VISTA database.

(B) Top: H3K27ac enrichment profiles showing predicted enhancers. Red bars indicate respective VISTA enhancer elements. Bottom: subregional cardiac enhancer activities of six VISTA heart enhancers that overlap iCLM enhancers. Shown is a representative transgenic E11.5 embryo with LacZ reporter staining (blue) indicating enhancer activity. Red arrowhead indicates the heart and heart sections that were counter-stained with Nuclear Fast Red. (white scale bars: 1 mm; black scale bars: 500 μm for whole-mount heart and 200 and 50 μm for low- and high-magnification histology sections, respectively)

(C and D) mRNA expression of *Gja5* (C) and *Tnni1* (D) is upregulated in day 2 iCLMs based on RNA-seq (n = 3 per group). Data are represented as mean ± SD.

(E) A highly conserved putative regulatory element ~25 kb downstream of the *Gja5* locus (Gja5-E) that overlaps with an ENCODE based candidate Regulatory Element (EM10E0224090) is co-occupied by TFs during cardiac reprogramming. Conservation track was generated from Euarchontoglires subset of the UCSC genome browser.

(F) Schematic of *Gja5* enhancer LacZ construct and a representative image of E11.5 transgenic embryo and heart stained with β-galactosidase showing LacZ expression in the heart. Numbers indicate embryos with cardiac expression over the total $LacZ^+$ genotyped embryos (white scale bar: 1 mm; black scale bar: 500 μm). A section of the E11.5 transgenic heart was counter-stained with Nuclear Fast Red (black scale bars: 200 and 50 μm for low-and high-magnification histology sections, respectively).

(G) A highly conserved putative regulatory element in the *Tnni1* intronic locus that overlaps with an ENCODE based candidate Regulatory Element (EM10E0347463) is co-occupied by TFs during cardiac reprogramming. The red dashed box indicates the region of the putative regulatory element.

(H) Schematic of *Tnni1* enhancer LacZ construct and a representative image of E11.5 transgenic embryo and heart stained with β-galactosidase showing LacZ expression in the heart. Numbers indicate embryos with cardiac expression over the total $LacZ^+$ genotyped embryos (white scale bar: 1 mm; black scale bar, 500 μm). A section of E11.5 transgenic heart was counter-stained with Nuclear Fast Red (Black scale bars, 200 and 50 μm for low- and high-magnification histology sections, respectively).

(I and J) Schematic of *Gja5* (I) and *Tnni1* (J) enhancer mCherry construct. *Gja5*-E- or *Tnni1*-E-Hsp68-mCherry was retrovirally delivered to MEFs together with the reprogramming factors. Representative image of day 7 mock-infected, GMT, GHMT, and AGHMT MEFs shows mCherry expression. (Bars, 50 μm.)

See also Figures S4 and S5, Table S4, and Table S5.

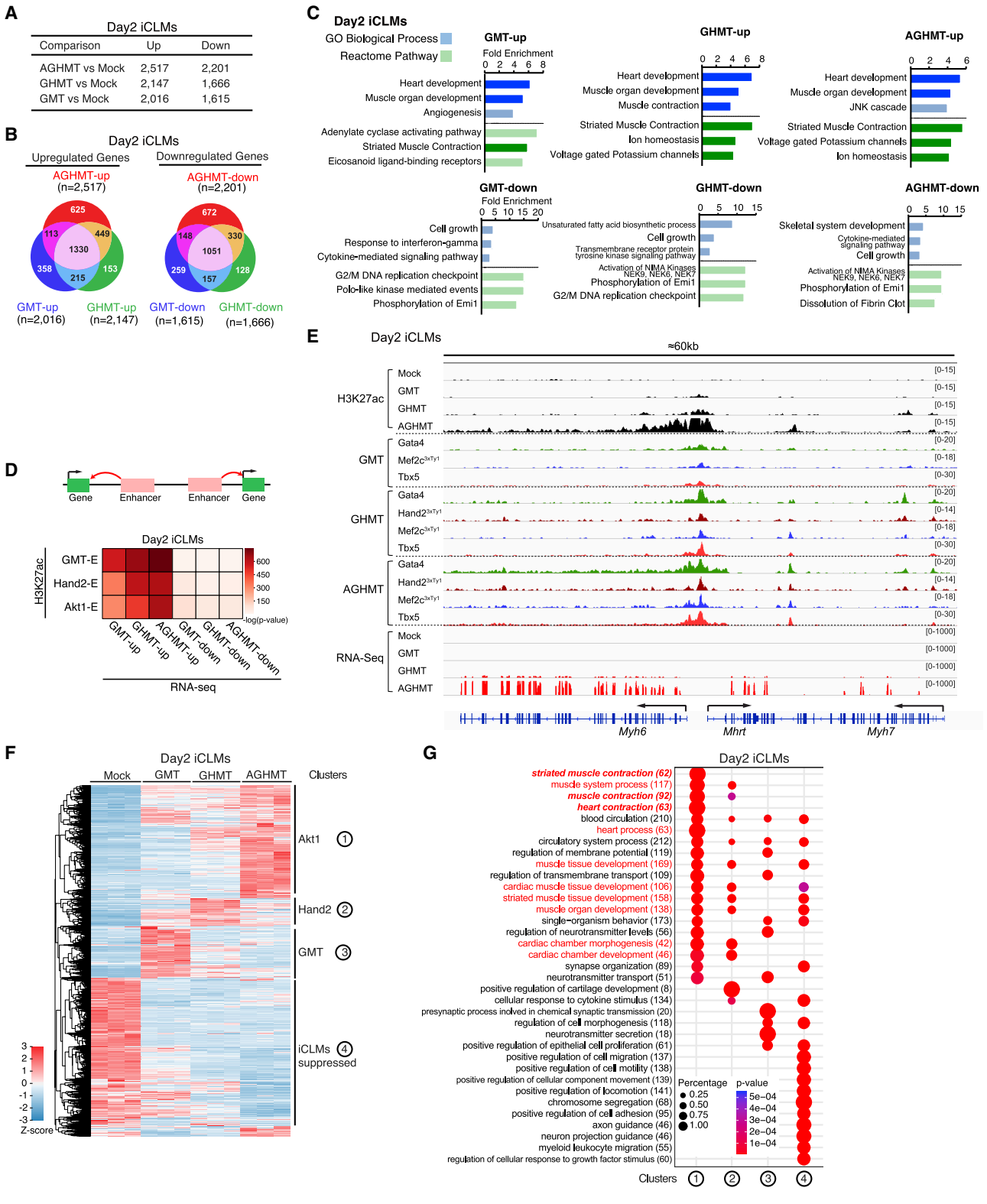

Figure 5. Reprogramming Enhancers Positively Correlate with Gene Upregulation during Cardiac Reprogramming

(A and B) Table (A) and Venn diagrams (B) displaying the number of common and unique genes upregulated and downregulated in GMT, GHMT, and AGHMT day 2 iCLMs compared to mock (n = 3 per group).

(legend continued on next page)

putative *Tnni1* enhancer (Tnni1-E) in the myocardium of multiple cardiac chambers at E11.5 and E13.5 (Figures 4H and S5B).

Additionally, we generated *Gja5*- and *Tnni1*-E-Hsp68-mCherry retroviral constructs to test enhancer activity during reprogramming. Retroviral delivery of these individual constructs along with reprogramming factors resulted in activation of mCherry expression in iCLMs, confirming that these enhancers are activated during reprogramming (Figures 4I, 4J, and S5C–S5G).

iCLM Transcriptional Modules Correlate with the Reprogramming Enhancer Landscape

To understand the correlation between reprogramming enhancers and gene expression profiles during reprogramming, we performed RNA sequencing (RNA-seq) on day 2 iCLMs. *In silico* analyses using PANTHER indicated that upregulated genes in GMT, GHMT, and AGHMT iCLMs compared to Mock (GMT-up, GHMT-up, and AGHMT-up) were associated with GO terms related to heart and muscle development, while downregulated genes (GMT-down, GHMT-down, and AGHMT-down) were associated with terms related to cell cycle (Mi et al., 2017) (Figures 5A–5C). To clarify the relationship between enhancer activation and transcriptional dynamics during reprogramming, we annotated the Reprogramming-E peaks to the nearest neighboring genes and calculated enrichment significance by hypergeometric distribution. This analysis revealed a significant correlation between Reprogramming-E peaks and upregulated genes in iCLMs, supporting the hypothesis that activation of enhancers by TF co-occupancy contributes to gene activation during reprogramming, and Hand2 and Akt1 enhance this process (Figure 5D). For example, Hand2- and Akt1-dependent activation of H3K27ac peaks near the *Myh6*, *Mhrt*, and *Myh7* locus is associated with their transcriptional upregulation in day 2 iCLMs (Figure 5E). We then performed global differential gene expression analyses in different iCLMs and clustered the genes uniquely responsive to GMT, Hand2, or Akt1 (Figure 5F). Consistent with previous reports of reprogramming enhancement by Hand2 and Akt1, *in silico* analyses revealed that Hand2- and Akt1-responsive genes displayed high enrichment in heart and muscle development and contraction-related GO terms (Figure 5G) (Song et al., 2012; Zhou et al., 2015).

We also performed RNA-seq on day 7 iCLMs to study the transcriptional dynamics during reprogramming. In agreement with delayed activation of cardiac enhancers annotated to functional phenotypes (Figure 2E), genes that were upregulated between day 2 and 7 showed significant enrichment in GO terms related to heart or muscle contraction, while downregulated genes were highly enriched in terms related to extracellular matrix (ECM) (Figure S6A). Additionally, approximately half of the genes in day 2 iCLM clusters 1 (Akt1) and 2 (Hand2) were upregulated in day 7 GHMT or GMT iCLMs, suggesting that Akt1 and Hand2 both enhance reprogramming by possibly inducing and accelerating unique gene expression (Figure S6B).

iCLM GRN Reveals Transcriptional Targets of Reprogramming Factors

We next investigated the relationship between transcriptional regulation by TFs in reprogramming and the heart *in vivo*. We performed ChIP-seq on P4 mouse ventricle for Gata4 and Tbx5 (GT) and compared the data with day 2 AGHMT iCLM GT peaks. Among the 33,409 iCLM GT peaks, 19,808 peaks were also bound by GT in the P4 ventricle, suggesting that certain reprogramming regulatory elements are also co-occupied by reprogramming factors *in vivo* (Figure 6A). However, iCLMs had 13,601 unique GT peaks, which could potentially be regulatory elements contributing to the reprogramming process. *In silico* analyses using GREAT showed enrichment of GO terms related to cardiac and muscle development and differentiation in the shared and P4 ventricle unique GT peaks (Figure 6B). In contrast, unique iCLM GT peaks showed enrichment of non-cardiac GO terms, which suggested that the role of reprogramming TFs in transcriptional regulation during reprogramming could differ from *in vivo* cardiac development.

Therefore, to study the cooperative actions of reprogramming TFs in transcriptional regulation during reprogramming, we decided to construct a GRN of reprogramming factors in day 2 AGHMT iCLMs. We first annotated all TF peaks (41,606) of day 2 AGHMT iCLMs in Figure 1B to their nearest neighboring genes and clustered the TF binding peaks depending on their target gene expression (Figure 6C). We then took the genes upregulated in day 2 AGHMT iCLMs compared to mock-infected MEFs and colored them according to their nearest TF peak to denote whether the activation was GMT (green), Hand2 (GHMT) (blue), or Akt1 (AGHMT) (red) dependent (Figure 6D). Finally, connecting each gene with reprogramming factors based on the TF peaks provided a GRN of reprogramming factors with their potential direct target genes during reprogramming (Figure 6E). Consistent with our finding of enhancer activation by co-occupancy, most of the upregulated genes were regulated by at least two reprogramming factors, with the largest numbers in GHMT (n = 700) and GHT (n = 332) groups (Table S6). *In silico* analysis using PANTHER showed that genes in the upregulated GRN were highly enriched in GO terms related to muscle contraction, metabolism, cell-cell interaction, and

(C) *In silico* functional annotation of day 2 iCLM gene sets performed using PANTHER, and the three most overrepresented GO Biological Process (blue) and Reactome Pathway (green) terms are shown. Terms related to heart or muscle are highlighted in dark colors.

(D) The enrichment significance of differentially expressed genes (columns) overlapping the reprogramming enhancer cluster (rows) in day 2 iCLMs was calculated using hypergeometric distribution.

(E) A genome browser view of the *Myh6*, *Mhrt*, and *Myh7* locus showing Hand2- and Akt1-dependent activation of H3K27ac peaks with TF co-occupancy, which is associated with mRNA upregulation in day 2 iCLMs.

(F) Heatmap of normalized FPKMs for all differentially expressed genes that meet inclusion criteria ($|\log2\ FC| \geq 1.0$, p value ≤ 0.01, false discovery rate [FDR] $\leq$ 1%) for GMT, GHMT, and AGHMT day 2 iCLMs compared to mock-infected MEFs.

(G) Genes from clusters corresponding to the numbers in (E) were used to perform GO enrichment analysis for Biological Process with DAVID (v.6.8). clusterProfiler (v.3.6.0) was used to visualize GO term enrichment. Terms related to heart or muscle are highlighted in red, and heart- or muscle-contraction-related terms are highlighted in red italics.

See also Figure S6.

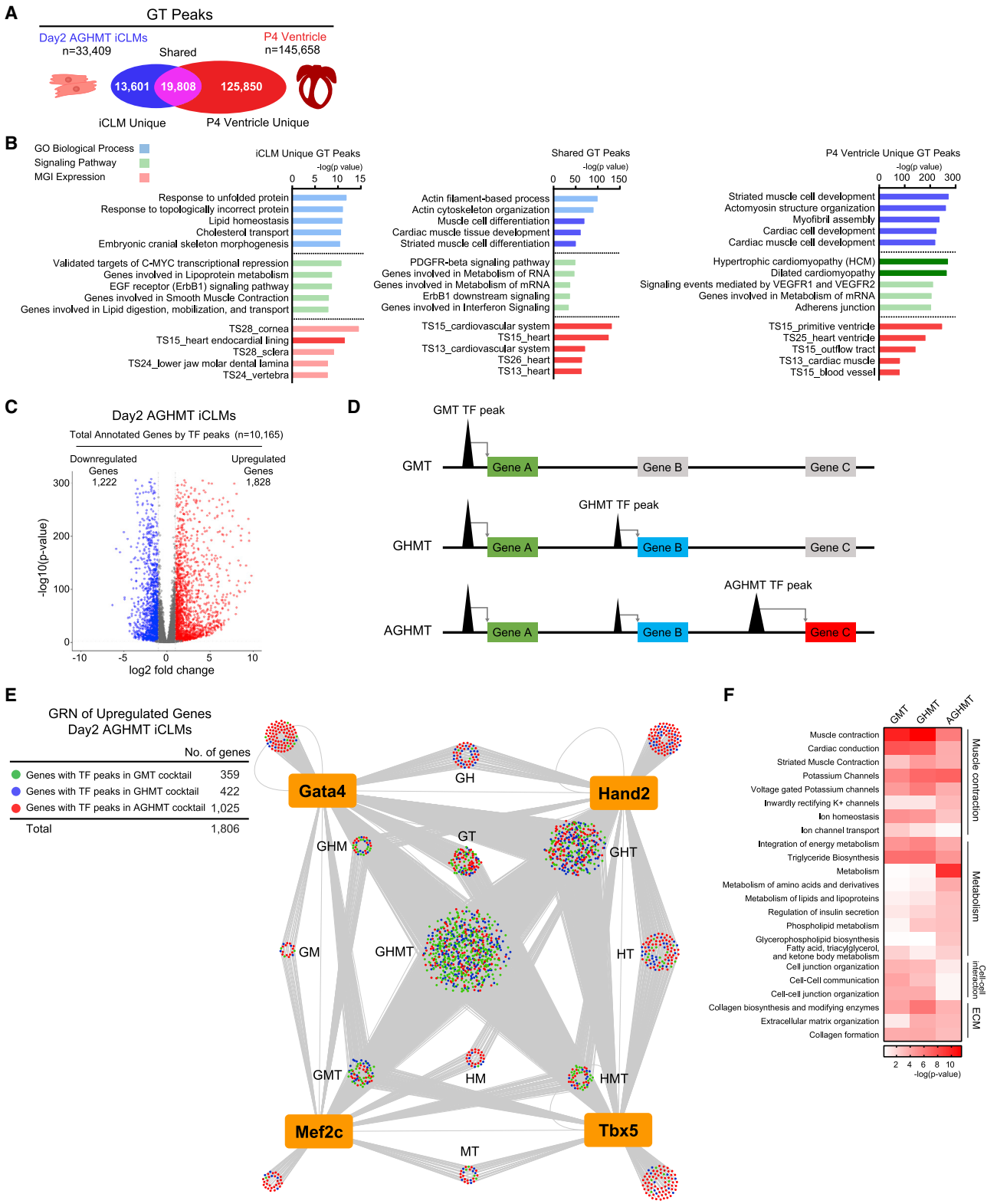

Figure 6. Construction of GRN during Cardiac Reprogramming

(A) Comparison of Gata4 and Tbx5 (GT) peaks between day 2 AGHMT iCLMs and P4 ventricle.

(B) *In silico* functional annotation using GREAT showing the five most overrepresented GO Biological Process (blue), Signaling Pathway (green), and MGI Expression (red) terms. Terms related to heart or muscle are highlighted in dark colors.

(legend continued on next page)

ECM, consistent with fibroblasts converting to a contracting muscle cell with high metabolic demand (Figure 6F).

We then constructed a GRN of downregulated genes in day 2 AGHMT iCLMs compared to mock-infected MEFs, which also showed that the largest number of genes were regulated by GHMT (n = 290) and GHT (n = 265) groups (Figure 7A; Table S6). Genes in the downregulated GRN showed high enrichment in GO terms related to the cell cycle, ECM, and inflammation pathways, which have been reported to enhance reprogramming by their suppression (Figures 7B, S7A, and S7B) (Liu et al., 2017; Zhao et al., 2015; Zhou et al., 2017). Additionally, in the downregulated GRN, we unexpectedly found enrichment of genes related to the EGF receptor (Egfr/Erbb1) signaling (Figures 7C and 7D). Interestingly, the Egfr signaling pathway was also shown to be enriched in our previous *in silico* analysis of iCLM unique and shared GT peaks (Figure 6B). Moreover, reprogramming TF peaks unique to AGHMT iCLMs were identified within the *Egfr* locus (Figure S7C). These peaks were associated with a dampening of H3K27ac signal, suggesting that ectopic binding of the reprogramming TFs in iCLMs may suppress *Egfr* expression (Figure S7C).

Based on these findings, we surmised that inhibiting the Egfr signaling pathway could enhance cardiac reprogramming. We tested the clinically utilized small-molecule tyrosine kinase inhibitor, Erlotinib, on iCLMs during reprogramming (Huang et al., 2012) (Figure 7E). Treatment with 5 μM Erlotinib enhanced the AGHMT reprogramming efficiency of MEFs, adult CFs, and tail-tip fibroblasts (TTFs) as measured by immunostaining of cardiac markers, Ca^{2+} flux, and spontaneous beating (Figures 7F–7I, S7D, and S7E; Video S1). To further assess the impact of Egfr signaling inhibition on reprogramming, we focused on *Jak2*, a gene identified in our downregulated GRN of Egfr signaling (Figures 7C and 7D). Although discrepancies were reported on the outcome of Jak inhibition in cardiac reprogramming, we surmised this could be due to differences in the reprogramming cocktails (Christoforou et al., 2013; Jayawardena et al., 2012; Moisan et al., 2015; Muraoka et al., 2014). Therefore, we tested another Jak inhibitor, Ruxolitinib, in our AGHMT reprogramming assay. Interestingly, treatment with 5 μM Ruxolitinib enhanced reprogramming efficiency by immunostaining to a similar degree but demonstrated increased Ca^{2+} flux and spontaneous beating compared to Erlotinib (Figures 7F–7I; Video S1). However, 5 μM Erlotinib and 5 μM Ruxolitinib together did not show synergistic effects, suggesting that enhancement by these chemicals shares some common signaling pathways (Figures 7F–7I). To confirm that the augmentation of reprogramming was not specific to these chemicals, we tested an alternative Egfr inhibitor, Gefitinib, and a Jak2 inhibitor, AZD1480, and demonstrated that both chemicals consistently augmented reprogramming of MEFs (Figures S7F and S7G). Additionally, we inhibited *Egfr* and *Jak2* expression by small hairpin RNAs, which also augmented reprogramming of MEFs (Figures 7J–7L, S7H, and S7I). In conclusion, GRN analysis revealed transcriptional networks directly regulated by reprogramming factors during cardiac reprogramming, and we identified the Egfr signaling pathway as a target to enhance the reprogramming process.

DISCUSSION

Cardiogenesis is known to be coordinated by combinatorial actions of multiple TFs, but the epigenomic regulation during cardiac reprogramming has not been previously investigated (He et al., 2011; Luna-Zurita et al., 2016). Here, we found that cardiogenic TFs function in a combinatorial manner by co-occupying myriad regulatory elements during the reprogramming process. In addition, our study highlights the importance of Mef2c in these combinatorial interactions for reprogramming (Wang et al., 2015). ChIP-seq analyses at the initial stage of reprogramming revealed that Gata4 and Tbx5 are recruited to Mef2 binding sites in reprogramming enhancers, where they work in concert for transcriptional activation. Consistently, reprogramming enhancers activated by Hand2 and Akt1 were also highly enriched with Mef2 motifs. These data suggest that cooperative actions of reprogramming TFs in the vicinity of Mef2 binding sites are crucial for cardiac reprogramming, and we propose that Mef2c is a protagonist in this process by recruiting reprogramming TFs to its binding sites. This notion also explains the failure of the Gata4, Hand2, and Tbx5 cocktail to reprogram fibroblasts into iCLMs, despite their synergistic transcriptional activities (Dai et al., 2002; Maitra et al., 2009).

Epigenetic Commonalities between Reprogramming and Cardiogenesis

Enhancers are major contributors to transcriptional divergence, based on their wide diversity among cell types and species (Chang and Bruneau, 2012; Gilsbach et al., 2018). Enhancer landscape commonalities between cardiac reprogramming and cellular differentiation reveal a biological link between these two cardiogenic processes. Considering that the reprogramming process is a direct cell-fate conversion by cardiogenic TFs, we were surprised to find an overlap between reprogramming enhancers and active enhancers in ESCs. The unexpected activation of these ESC enhancers provides new insights into the epigenetic function of reprogramming TFs and may explain why small molecules or growth factors involved in cardiac differentiation from pluripotent stem cells augment reprogramming (Abad et al., 2017; Yamakawa et al., 2015).

(C) Volcano plot of all differentially expressed genes annotated by day 2 AGHMT iCLMs TF peaks. Genes with their expression increased or decreased greater than 2-fold in AGHMT iCLMs compared to mock-infected MEFs with p value <0.01 are colored in red and blue, respectively.

(D) Strategy for constructing GRN. Genes were colored according to their nearest TF peaks, if the peak activation was GMT (green), Hand2 (GHMT) (blue), or Akt1 (AGHMT) (red) dependent.

(E) GRN of reprogramming factors and upregulated genes in day 2 AGHMT iCLMs. Each node represents a gene and edges are drawn to all the annotated genes of reprogramming TF peaks.

(F) Genes colored in green (GMT), blue (Hand2), or red (Akt1) in (E) were used in GO analyses using PANTHER. Heatmap shows upregulated signaling pathways targeted by reprogramming factors.

See also Table S6.

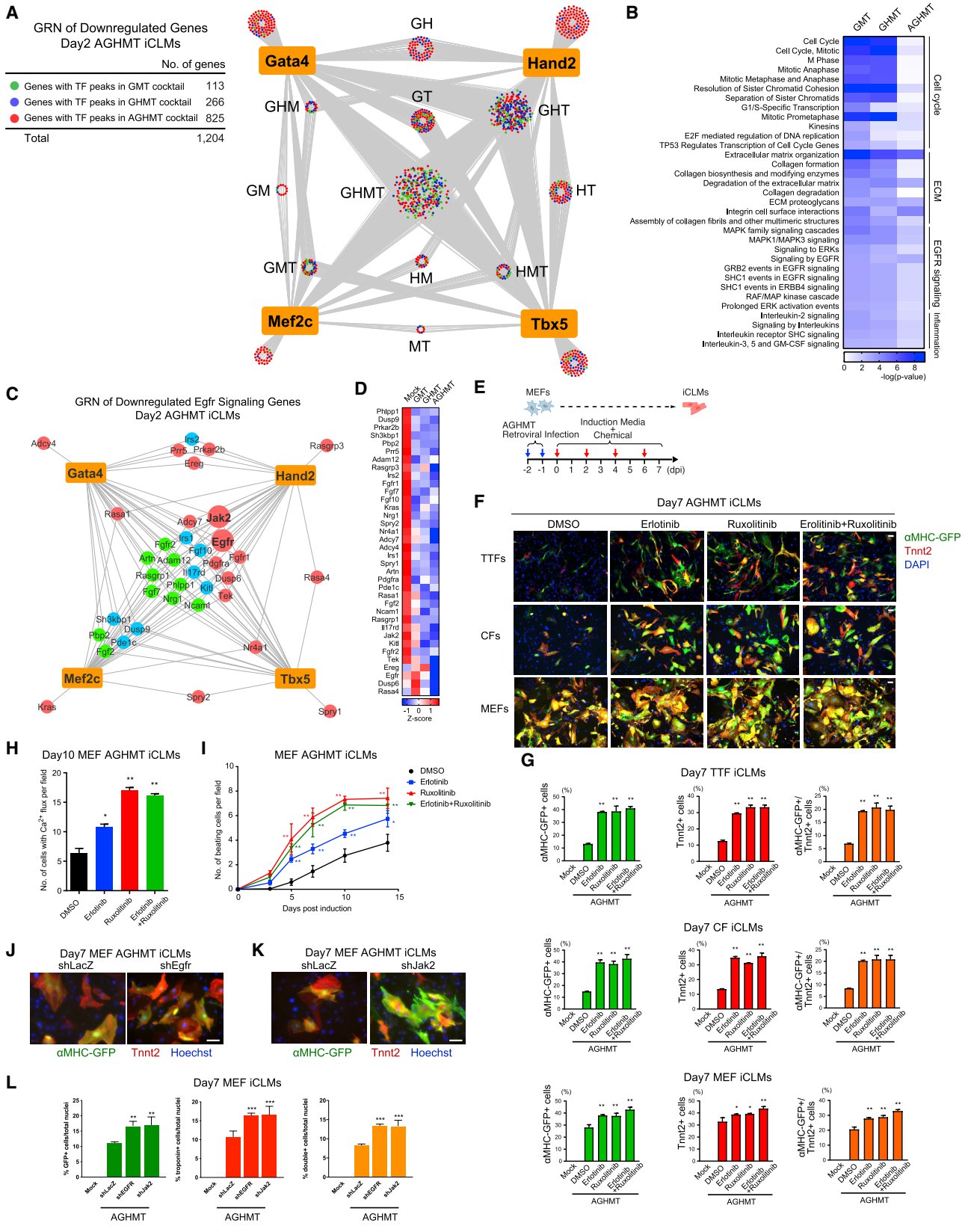

(legend on next page)

The early iCLM enhancer landscape was most similar to that of the neonatal heart among different developmental stages. However, we demonstrated that maturation enhancers are subsequently activated in iCLMs at a later time point (day 7), and the addition of Hand2 and Akt1 further augmented this process. These findings suggest that activation of maturation enhancers is essential for iCLMs to acquire a more functional phenotype. Furthermore, Mef2c plays a key role in this process, as demonstrated by the enrichment of its binding site in these enhancer regions. Thus, our study highlights the impact of enhancer activation in cardiac reprogramming and defines factors that can activate maturation enhancers and thereby produce more mature iCLMs.

Egfr Signaling Inhibits Reprogramming

GRN analysis enabled the identification of Egfr signaling as an inhibitory pathway of reprogramming. Considering the therapeutic potential of the reprogramming approach, we verified the inhibitory action of Egfr signaling by applying short hairpin RNA (shRNA) and already clinically available chemicals (Kobayashi and Hagiwara, 2013; Vannucchi et al., 2015). Although the precise mechanism has yet to be determined, since Egfr inhibition is known to enhance cardiac differentiation from pluripotent stem cells, the unpredicted activation of ESC enhancers in iCLMs may account for its action (Ramachandra et al., 2016).

Summary

In conclusion, our genome-wide study reveals a transition of enhancer landscape and gene expression during cardiac reprogramming, which is orchestrated by cooperative TF function. However, the immaturity of iCLMs indicates additional processes required for full activation of a cardiac enhancer landscape. Considering the therapeutic potential of direct cardiac reprogramming, it will be interesting to dissect the epigenetic landscape of cardiac reprogramming in human cells, as reprogramming factors differ between mouse and human fibroblasts (Fu et al., 2013; Nam et al., 2013; Wada et al., 2013). Such information may explain why additional factors are required to reprogram human fibroblasts into CMs and provide new insights into human reprogramming thereby advancing the field for regenerative therapy.

STAR★METHODS

Detailed methods are provided in the online version of this paper and include the following:

- KEY RESOURCES TABLE
- CONTACT FOR REAGENT AND RESOURCE SHARING
- EXPERIMENTAL MODEL AND SUBJECT DETAILS
  - Cell lines
  - Mice
- METHOD DETAILS
  - Cell culture
  - Retrovirus production and cardiac reprogramming
  - Quantitative mRNA measurement
  - Immunocytochemistry
  - Western blot analyses
  - Flow cytometry
  - Beating cell analysis and calcium assay
  - *In vitro* and *in vivo* transgenic reporter assays
  - ChIP-seq sample preparation
  - RNA-seq sample preparation
- QUANTIFICATION AND STATISTICAL ANALYSIS
  - ChIP-seq analysis
  - RNA-seq analysis
  - Gene regulatory network analysis
  - Statistical analysis
- DATA AND SOFTWARE AVAILABILITY

SUPPLEMENTAL INFORMATION

Supplemental Information can be found online at https://doi.org/10.1016/j.stem.2019.03.022.

ACKNOWLEDGMENTS

We thank J. Cabrera for graphical assistance; J. McAnally for performing microinjection for the in vivo transgenic reporter assay; J. Richardson,

Figure 7. Inhibition of EGFR Signaling Enhances Cardiac Reprogramming

(A) GRN of reprogramming factors and downregulated genes in day 2 AGHMT iCLMs. Each node represents a gene and edges are drawn to all the annotated genes of reprogramming TF peaks.

(B) Genes colored in green (GMT), blue (Hand2), or red (Akt1) in (A) were used for GO analyses using PANTHER. Heatmap shows downregulated signaling pathways targeted by reprogramming factors.

(C) GRN of downregulated Egfr signaling pathway genes in day 2 AGHMT iCLMs.

(D) Gene expression heatmap of all genes from (C).

(E) Strategy for testing chemicals on iCLMs during reprogramming.

(F) Representative immunocytochemistry images of AGHMT reprogrammed fibroblasts from αMHC-GFP transgenic mice treated with DMSO or the indicated chemicals. Cells were fixed and stained for αMHC-GFP (green), Tnnt2 (red), and DAPI (blue) 7 days after infection. (Bars, 100 μm.)

(G) Quantification by flow cytometry of αMHC-GFP$^+$ and Tnnt2$^+$ iCLMs 7 days after treatment with AGHMT and DMSO or the indicated chemicals (n = 3, independent experiments). (*p < 0.05 versus AGHMT+DMSO, **p < 0.01 versus AGHMT+DMSO.) Data are represented as mean ± SD.

(H) Quantification of Ca^{2+} flux-positive MEFs after 10 days of reprogramming using Fluo-4 NW dye (n = 3, independent experiments). (*p < 0.05 versus AGHMT+DMSO, **p < 0.01 versus AGHMT+DMSO). Data are represented as mean ± SD.

(I) Quantification of spontaneous beating MEF iCLMs after treatment (n = 3, independent experiments). (*p < 0.05 versus AGHMT+DMSO, **p < 0.01 versus AGHMT+DMSO.) Data are represented as mean ± SD.

(J and K) Representative immunocytochemistry images of AGHMT iCLMs from αMHC-GFP transgenic mice treated with Egfr shRNA (J) or Jak2 shRNA (K). Cells were fixed and stained for αMHC-GFP (green), Tnnt2 (red), and Hoechst (blue) 7 days after infection. (Bars, 100 μm.)

(L) Quantification of αMHC-GFP$^+$ and Tnnt2$^+$ iCLMs 7 days after infection with AGHMT and the indicated shRNAs by immunocytochemistry (n = 3, independent experiments). (**p < 0.01 versus AGHMT+shLacZ, ***p < 0.0001 versus AGHMT+shLacZ.) Data are represented as mean ± SD.

See also Figure S7 and Table S6.

J. Shelton, and the UT Southwestern Histology Core for help with histopathology; and J. Xu, X. Liu, and the Sequencing Core Facility at Children's Research Institute and the Genomics and Microarray Core Facility at UT Southwestern for performing the Illumina sequencing. We are grateful to M.S. Kim for advice about the bioinformatics analysis. This work was supported by grants from the NIH (AR-067294, HL-130253, and HL-138426), Fondation Leducq Transatlantic Networks of Excellence in Cardiovascular Research, and the Robert A. Welch Foundation (grant 1-0025 to E.N.O.). H.H. was supported by a Uehara Memorial Foundation Postdoctoral Fellowship and a Kanae Foreign Study Grant. Z.W. was supported by a predoctoral fellowship from the American Heart Association (19PRE34380436). G.A.G. was supported by an NIH T32 Training grant (5T32HL125247-04). V.S.M was supported by Cancer Prevention and Research Institute of Texas (RP150596). Research by M.O., D.E.D., and A.V. was conducted at the E.O. Lawrence Berkeley National Laboratory and performed under Department of Energy Contract DE-AC02-05CH11231, University of California. The work was supported by NHLBI grant R24HL123879 (to A.V.). We thank the ENCODE Consortium and the ENCODE production laboratories for generating the particular datasets.

AUTHOR CONTRIBUTIONS

H.H., Z.W., G.A.G., V.S.M., G.A.B., W.Y., and H.Z. designed and performed experiments and contributed to data analysis, discussion, and writing; M.O., D.E.D., and A.V. contributed to experimental work and discussion; N.L. and R.B.-D. contributed to discussion and writing; and E.N.O. supervised the study and contributed to discussion and writing.

DECLARATION OF INTERESTS

E.N.O. is a cofounder and member of the Scientific Advisory Board of Tenaya Therapeutics and holds equity in the company. The other authors declare no competing interests.

Received: March 26, 2018
Revised: September 7, 2018
Accepted: March 25, 2019
Published: May 9, 2019

REFERENCES

Abad, M., Hashimoto, H., Zhou, H., Morales, M.G., Chen, B., Bassel-Duby, R., and Olson, E.N. (2017). Notch Inhibition Enhances Cardiac Reprogramming by Increasing MEF2C Transcriptional Activity. Stem Cell Reports *8*, 548–560.

Addis, R.C., Ifkovits, J.L., Pinto, F., Kellam, L.D., Esteso, P., Rentschler, S., Christoforou, N., Epstein, J.A., and Gearhart, J.D. (2013). Optimization of direct fibroblast reprogramming to cardiomyocytes using calcium activity as a functional measure of success. J. Mol. Cell. Cardiol. *60*, 97–106.

Ang, Y.S., Rivas, R.N., Ribeiro, A.J.S., Srivas, R., Rivera, J., Stone, N.R., Pratt, K., Mohamed, T.M.A., Fu, J.D., Spencer, C.I., et al. (2016). Disease Model of GATA4 Mutation Reveals Transcription Factor Cooperativity in Human Cardiogenesis. Cell *167*, 1734–1749.

Bagwe, S., Berenfeld, O., Vaidya, D., Morley, G.E., and Jalife, J. (2005). Altered right atrial excitation and propagation in connexin40 knockout mice. Circulation *112*, 2245–2253.

Blow, M.J., McCulley, D.J., Li, Z., Zhang, T., Akiyama, J.A., Holt, A., Plajzer-Frick, I., Shoukry, M., Wright, C., Chen, F., et al. (2010). ChIP-Seq identification of weakly conserved heart enhancers. Nat. Genet. *42*, 806–810.

Chang, C.P., and Bruneau, B.G. (2012). Epigenetics and cardiovascular development. Annu. Rev. Physiol. *74*, 41–68.

Christoforou, N., Chellappan, M., Adler, A.F., Kirkton, R.D., Wu, T., Addis, R.C., Bursac, N., and Leong, K.W. (2013). Transcription factors MYOCD, SRF, Mesp1 and SMARCD3 enhance the cardio-inducing effect of GATA4, TBX5, and MEF2C during direct cellular reprogramming. PLoS ONE *8*, e63577.

Cohn, J.N., Ferrari, R., and Sharpe, N. (2000). Cardiac remodeling–concepts and clinical implications: a consensus paper from an international forum on cardiac remodeling. Behalf of an International Forum on Cardiac Remodeling. J. Am. Coll. Cardiol. *35*, 569–582.

Condorelli, G., Drusco, A., Stassi, G., Bellacosa, A., Roncarati, R., Iaccarino, G., Russo, M.A., Gu, Y., Dalton, N., Chung, C., et al. (2002). Akt induces enhanced myocardial contractility and cell size in vivo in transgenic mice. Proc. Natl. Acad. Sci. USA *99*, 12333–12338.

Consortium, E.P.; ENCODE Project Consortium (2012). An integrated encyclopedia of DNA elements in the human genome. Nature *489*, 57–74.

Corin, S.J., Juhasz, O., Zhu, L., Conley, P., Kedes, L., and Wade, R. (1994). Structure and expression of the human slow twitch skeletal muscle troponin I gene. J. Biol. Chem. *269*, 10651–10659.

Creyghton, M.P., Cheng, A.W., Welstead, G.G., Kooistra, T., Carey, B.W., Steine, E.J., Hanna, J., Lodato, M.A., Frampton, G.M., Sharp, P.A., et al. (2010). Histone H3K27ac separates active from poised enhancers and predicts developmental state. Proc. Natl. Acad. Sci. USA *107*, 21931–21936.

Dai, Y.S., Cserjesi, P., Markham, B.E., and Molkentin, J.D. (2002). The transcription factors GATA4 and dHAND physically interact to synergistically activate cardiac gene expression through a p300-dependent mechanism. J. Biol. Chem. *277*, 24390–24398.

Dickel, D.E., Barozzi, I., Zhu, Y., Fukuda-Yuzawa, Y., Osterwalder, M., Mannion, B.J., May, D., Spurrell, C.H., Plajzer-Frick, I., Pickle, C.S., et al. (2016). Genome-wide compendium and functional assessment of in vivo heart enhancers. Nat. Commun. *7*, 12923.

Feng, J., Liu, T., Qin, B., Zhang, Y., and Liu, X.S. (2012). Identifying ChIP-seq enrichment using MACS. Nat. Protoc. *7*, 1728–1740.

Fu, J.D., Stone, N.R., Liu, L., Spencer, C.I., Qian, L., Hayashi, Y., Delgado-Olguin, P., Ding, S., Bruneau, B.G., and Srivastava, D. (2013). Direct reprogramming of human fibroblasts toward a cardiomyocyte-like state. Stem Cell Reports *1*, 235–247.

Fu, Y., Huang, C., Xu, X., Gu, H., Ye, Y., Jiang, C., Qiu, Z., and Xie, X. (2015). Direct reprogramming of mouse fibroblasts into cardiomyocytes with chemical cocktails. Cell Res. *25*, 1013–1024.

Galdos, F.X., Guo, Y., Paige, S.L., VanDusen, N.J., Wu, S.M., and Pu, W.T. (2017). Cardiac Regeneration: Lessons From Development. Circ. Res. *120*, 941–959.

Gilsbach, R., Schwaderer, M., Preissl, S., Grüning, B.A., Kranzhöfer, D., Schneider, P., Nührenberg, T.G., Mulero-Navarro, S., Weichenhan, D., Braun, C., et al. (2018). Distinct epigenetic programs regulate cardiac myocyte development and disease in the human heart in vivo. Nat. Commun. *9*, 391.

Harvey, R.P. (2002). Patterning the vertebrate heart. Nat. Rev. Genet. *3*, 544–556.

Hashimoto, H., Olson, E.N., and Bassel-Duby, R. (2018). Therapeutic approaches for cardiac regeneration and repair. Nat. Rev. Cardiol. *15*, 585–600.

He, A., Kong, S.W., Ma, Q., and Pu, W.T. (2011). Co-occupancy by multiple cardiac transcription factors identifies transcriptional enhancers active in heart. Proc. Natl. Acad. Sci. USA *108*, 5632–5637.

Heinz, S., Benner, C., Spann, N., Bertolino, E., Lin, Y.C., Laslo, P., Cheng, J.X., Murre, C., Singh, H., and Glass, C.K. (2010). Simple combinations of lineage-determining transcription factors prime cis-regulatory elements required for macrophage and B cell identities. Mol. Cell *38*, 576–589.

Heinz, S., Romanoski, C.E., Benner, C., and Glass, C.K. (2015). The selection and function of cell type-specific enhancers. Nat. Rev. Mol. Cell Biol. *16*, 144–154.

Huang, W., Sherman, B.T., and Lempicki, R.A. (2009a). Bioinformatics enrichment tools: paths toward the comprehensive functional analysis of large gene lists. Nucleic Acids Res. *37*, 1–13.

Huang, W., Sherman, B.T., and Lempicki, R.A. (2009b). Systematic and integrative analysis of large gene lists using DAVID bioinformatics resources. Nat. Protoc. *4*, 44–57.

Huang, S., Hölzel, M., Knijnenburg, T., Schlicker, A., Roepman, P., McDermott, U., Garnett, M., Grernrum, W., Sun, C., Prahallad, A., et al. (2012). MED12 controls the response to multiple cancer drugs through regulation of TGF-β receptor signaling. Cell *151*, 937–950.

Huang, J., Liu, X., Li, D., Shao, Z., Cao, H., Zhang, Y., Trompouki, E., Bowman, T.V., Zon, L.I., Yuan, G.C., et al. (2016). Dynamic Control of Enhancer

Repertoires Drives Lineage and Stage-Specific Transcription during Hematopoiesis. Dev. Cell *36*, 9–23.

Ieda, M., Fu, J.D., Delgado-Olguin, P., Vedantham, V., Hayashi, Y., Bruneau, B.G., and Srivastava, D. (2010). Direct reprogramming of fibroblasts into functional cardiomyocytes by defined factors. Cell *142*, 375–386.

Jahangiri, L., Sharpe, M., Novikov, N., González-Rosa, J.M., Borikova, A., Nevis, K., Paffett-Lugassy, N., Zhao, L., Adams, M., Guner-Ataman, B., et al. (2016). The AP-1 transcription factor component Fosl2 potentiates the rate of myocardial differentiation from the zebrafish second heart field. Development *143*, 113–122.

Jayawardena, T.M., Egemnazarov, B., Finch, E.A., Zhang, L., Payne, J.A., Pandya, K., Zhang, Z., Rosenberg, P., Mirotsou, M., and Dzau, V.J. (2012). MicroRNA-mediated in vitro and in vivo direct reprogramming of cardiac fibroblasts to cardiomyocytes. Circ. Res. *110*, 1465–1473.

Kharchenko, P.V., Tolstorukov, M.Y., and Park, P.J. (2008). Design and analysis of ChIP-seq experiments for DNA-binding proteins. Nat. Biotechnol. *26*, 1351–1359.

King, A.D., Huang, K., Rubbi, L., Liu, S., Wang, C.Y., Wang, Y., Pellegrini, M., and Fan, G. (2016). Reversible Regulation of Promoter and Enhancer Histone Landscape by DNA Methylation in Mouse Embryonic Stem Cells. Cell Rep. *17*, 289–302.

Kobayashi, K., and Hagiwara, K. (2013). Epidermal growth factor receptor (EGFR) mutation and personalized therapy in advanced nonsmall cell lung cancer (NSCLC). Target. Oncol. *8*, 27–33.

Kothary, R., Clapoff, S., Darling, S., Perry, M.D., Moran, L.A., and Rossant, J. (1989). Inducible expression of an hsp68-lacZ hybrid gene in transgenic mice. Development *105*, 707–714.

Lalit, P.A., Salick, M.R., Nelson, D.O., Squirrell, J.M., Shafer, C.M., Patel, N.G., Saeed, I., Schmuck, E.G., Markandeya, Y.S., Wong, R., et al. (2016). Lineage Reprogramming of Fibroblasts into Proliferative Induced Cardiac Progenitor Cells by Defined Factors. Cell Stem Cell *18*, 354–367.

Landt, S.G., Marinov, G.K., Kundaje, A., Kheradpour, P., Pauli, F., Batzoglou, S., Bernstein, B.E., Bickel, P., Brown, J.B., Cayting, P., et al. (2012). ChIP-seq guidelines and practices of the ENCODE and modENCODE consortia. Genome Res. *22*, 1813–1831.

Laurent, F., Girdziusaite, A., Gamart, J., Barozzi, I., Osterwalder, M., Akiyama, J.A., Lincoln, J., Lopez-Rios, J., Visel, A., Zuniga, A., and Zeller, R. (2017). HAND2 Target Gene Regulatory Networks Control Atrioventricular Canal and Cardiac Valve Development. Cell Rep. *19*, 1602–1613.

Li, H., and Durbin, R. (2009). Fast and accurate short read alignment with Burrows-Wheeler transform. Bioinformatics *25*, 1754–1760.

Li, H., Handsaker, B., Wysoker, A., Fennell, T., Ruan, J., Homer, N., Marth, G., Abecasis, G., and Durbin, R.; 1000 Genome Project Data Processing Subgroup (2009). The Sequence Alignment/Map format and SAMtools. Bioinformatics *25*, 2078–2079.

Liao, Y., Smyth, G.K., and Shi, W. (2014). featureCounts: an efficient general purpose program for assigning sequence reads to genomic features. Bioinformatics *30*, 923–930.

Liu, N., Williams, A.H., Kim, Y., McAnally, J., Bezprozvannaya, S., Sutherland, L.B., Richardson, J.A., Bassel-Duby, R., and Olson, E.N. (2007). An intragenic MEF2-dependent enhancer directs muscle-specific expression of microRNAs 1 and 133. Proc. Natl. Acad. Sci. USA *104*, 20844–20849.

Liu, Z., Wang, L., Welch, J.D., Ma, H., Zhou, Y., Vaseghi, H.R., Yu, S., Wall, J.B., Alimohamadi, S., Zheng, M., et al. (2017). Single-cell transcriptomics reconstructs fate conversion from fibroblast to cardiomyocyte. Nature *551*, 100–104.

Luna-Zurita, L., Stirnimann, C.U., Glatt, S., Kaynak, B.L., Thomas, S., Baudin, F., Samee, M.A., He, D., Small, E.M., Mileikovsky, M., et al. (2016). Complex Interdependence Regulates Heterotypic Transcription Factor Distribution and Coordinates Cardiogenesis. Cell *164*, 999–1014.

Maitra, M., Schluterman, M.K., Nichols, H.A., Richardson, J.A., Lo, C.W., Srivastava, D., and Garg, V. (2009). Interaction of Gata4 and Gata6 with Tbx5 is critical for normal cardiac development. Dev. Biol. *326*, 368–377.

McLean, C.Y., Bristor, D., Hiller, M., Clarke, S.L., Schaar, B.T., Lowe, C.B., Wenger, A.M., and Bejerano, G. (2010). GREAT improves functional interpretation of cis-regulatory regions. Nat. Biotechnol. *28*, 495–501.

Mi, H., Huang, X., Muruganujan, A., Tang, H., Mills, C., Kang, D., and Thomas, P.D. (2017). PANTHER version 11: expanded annotation data from Gene Ontology and Reactome pathways, and data analysis tool enhancements. Nucleic Acids Res. *45* (D1), D183–D189.

Mohamed, T.M., Stone, N.R., Berry, E.C., Radzinsky, E., Huang, Y., Pratt, K., Ang, Y.S., Yu, P., Wang, H., Tang, S., et al. (2017). Chemical Enhancement of In Vitro and In Vivo Direct Cardiac Reprogramming. Circulation *135*, 978–995.

Moisan, A., Lee, Y.K., Zhang, J.D., Hudak, C.S., Meyer, C.A., Prummer, M., Zoffmann, S., Truong, H.H., Ebeling, M., Kiialainen, A., et al. (2015). White-to-brown metabolic conversion of human adipocytes by JAK inhibition. Nat. Cell Biol. *17*, 57–67.

Morin, S., Charron, F., Robitaille, L., and Nemer, M. (2000). GATA-dependent recruitment of MEF2 proteins to target promoters. EMBO J. *19*, 2046–2055.

Morisco, C., Seta, K., Hardt, S.E., Lee, Y., Vatner, S.F., and Sadoshima, J. (2001). Glycogen synthase kinase 3beta regulates GATA4 in cardiac myocytes. J. Biol. Chem. *276*, 28586–28597.

Mudge, J.M., and Harrow, J. (2015). Creating reference gene annotation for the mouse C57BL6/J genome assembly. Mamm. Genome *26*, 366–378.

Muraoka, N., Yamakawa, H., Miyamoto, K., Sadahiro, T., Umei, T., Isomi, M., Nakashima, H., Akiyama, M., Wada, R., Inagawa, K., et al. (2014). MiR-133 promotes cardiac reprogramming by directly repressing Snai1 and silencing fibroblast signatures. EMBO J. *33*, 1565–1581.

Nam, Y.J., Song, K., Luo, X., Daniel, E., Lambeth, K., West, K., Hill, J.A., DiMaio, J.M., Baker, L.A., Bassel-Duby, R., and Olson, E.N. (2013). Reprogramming of human fibroblasts toward a cardiac fate. Proc. Natl. Acad. Sci. USA *110*, 5588–5593.

Nam, Y.J., Lubczyk, C., Bhakta, M., Zang, T., Fernandez-Perez, A., McAnally, J., Bassel-Duby, R., Olson, E.N., and Munshi, N.V. (2014). Induction of diverse cardiac cell types by reprogramming fibroblasts with cardiac transcription factors. Development *141*, 4267–4278.

Olson, E.N. (2006). Gene regulatory networks in the evolution and development of the heart. Science *313*, 1922–1927.

Pertea, M., Kim, D., Pertea, G.M., Leek, J.T., and Salzberg, S.L. (2016). Transcript-level expression analysis of RNA-seq experiments with HISAT, StringTie and Ballgown. Nat. Protoc. *11*, 1650–1667.

Quinlan, A.R., and Hall, I.M. (2010). BEDTools: a flexible suite of utilities for comparing genomic features. Bioinformatics *26*, 841–842.

Ramachandra, C.J., Mehta, A., Lua, C.H., Chitre, A., Ja, K.P., and Shim, W. (2016). ErbB Receptor Tyrosine Kinase: A Molecular Switch Between Cardiac and Neuroectoderm Specification in Human Pluripotent Stem Cells. Stem Cells *34*, 2461–2470.

Ramírez, F., Ryan, D.P., Grüning, B., Bhardwaj, V., Kilpert, F., Richter, A.S., Heyne, S., Dündar, F., and Manke, T. (2016). deepTools2: a next generation web server for deep-sequencing data analysis. Nucleic Acids Res. *44*, W160–W165.

Roth, G.A., Johnson, C., Abajobir, A., Abd-Allah, F., Abera, S.F., Abyu, G., Ahmed, M., Aksut, B., Alam, T., Alam, K., et al. (2017). Global, Regional, and National Burden of Cardiovascular Diseases for 10 Causes, 1990 to 2015. J. Am. Coll. Cardiol. *70*, 1–25.

Song, K., Nam, Y.J., Luo, X., Qi, X., Tan, W., Huang, G.N., Acharya, A., Smith, C.L., Tallquist, M.D., Neilson, E.G., et al. (2012). Heart repair by reprogramming non-myocytes with cardiac transcription factors. Nature *485*, 599–604.

Spitz, F., and Furlong, E.E. (2012). Transcription factors: from enhancer binding to developmental control. Nat. Rev. Genet. *13*, 613–626.

Takahashi, K., and Yamanaka, S. (2006). Induction of pluripotent stem cells from mouse embryonic and adult fibroblast cultures by defined factors. Cell *126*, 663–676.

Tarasov, A., Vilella, A.J., Cuppen, E., Nijman, I.J., and Prins, P. (2015). Sambamba: fast processing of NGS alignment formats. Bioinformatics *31*, 2032–2034.

Vannucchi, A.M., Kiladjian, J.J., Griesshammer, M., Masszi, T., Durrant, S., Passamonti, F., Harrison, C.N., Pane, F., Zachee, P., Mesa, R., et al. (2015). Ruxolitinib versus standard therapy for the treatment of polycythemia vera. N. Engl. J. Med. *372*, 426–435.

Visel, A., Minovitsky, S., Dubchak, I., and Pennacchio, L.A. (2007). VISTA Enhancer Browser–a database of tissue-specific human enhancers. Nucleic Acids Res. *35*, D88–D92.

Wada, R., Muraoka, N., Inagawa, K., Yamakawa, H., Miyamoto, K., Sadahiro, T., Umei, T., Kaneda, R., Suzuki, T., Kamiya, K., et al. (2013). Induction of human cardiomyocyte-like cells from fibroblasts by defined factors. Proc. Natl. Acad. Sci. USA *110*, 12667–12672.

Wamstad, J.A., Alexander, J.M., Truty, R.M., Shrikumar, A., Li, F., Eilertson, K.E., Ding, H., Wylie, J.N., Pico, A.R., Capra, J.A., et al. (2012). Dynamic and coordinated epigenetic regulation of developmental transitions in the cardiac lineage. Cell *151*, 206–220.

Wang, H., Cao, N., Spencer, C.I., Nie, B., Ma, T., Xu, T., Zhang, Y., Wang, X., Srivastava, D., and Ding, S. (2014). Small molecules enable cardiac reprogramming of mouse fibroblasts with a single factor, Oct4. Cell Rep. *6*, 951–960.

Wang, L., Liu, Z., Yin, C., Asfour, H., Chen, O., Li, Y., Bursac, N., Liu, J., and Qian, L. (2015). Stoichiometry of Gata4, Mef2c, and Tbx5 influences the efficiency and quality of induced cardiac myocyte reprogramming. Circ. Res. *116*, 237–244.

Xu, J., Shao, Z., Glass, K., Bauer, D.E., Pinello, L., Van Handel, B., Hou, S., Stamatoyannopoulos, J.A., Mikkola, H.K., Yuan, G.C., and Orkin, S.H. (2012). Combinatorial assembly of developmental stage-specific enhancers controls gene expression programs during human erythropoiesis. Dev. Cell *23*, 796–811.

Yamakawa, H., Muraoka, N., Miyamoto, K., Sadahiro, T., Isomi, M., Haginiwa, S., Kojima, H., Umei, T., Akiyama, M., Kuishi, Y., et al. (2015). Fibroblast Growth Factors and Vascular Endothelial Growth Factor Promote Cardiac Reprogramming under Defined Conditions. Stem Cell Reports *5*, 1128–1142.

Yoshida, T. (2008). MCAT elements and the TEF-1 family of transcription factors in muscle development and disease. Arterioscler. Thromb. Vasc. Biol. *28*, 8–17.

Yu, G., Wang, L.G., Han, Y., and He, Q.Y. (2012). clusterProfiler: an R package for comparing biological themes among gene clusters. OMICS *16*, 284–287.

Zhao, Y., Londono, P., Cao, Y., Sharpe, E.J., Proenza, C., O'Rourke, R., Jones, K.L., Jeong, M.Y., Walker, L.A., Buttrick, P.M., et al. (2015). High-efficiency reprogramming of fibroblasts into cardiomyocytes requires suppression of pro-fibrotic signalling. Nat. Commun. *6*, 8243.

Zhou, H., Dickson, M.E., Kim, M.S., Bassel-Duby, R., and Olson, E.N. (2015). Akt1/protein kinase B enhances transcriptional reprogramming of fibroblasts to functional cardiomyocytes. Proc. Natl. Acad. Sci. USA *112*, 11864–11869.

Zhou, H., Morales, M.G., Hashimoto, H., Dickson, M.E., Song, K., Ye, W., Kim, M.S., Niederstrasser, H., Wang, Z., Chen, B., et al. (2017). ZNF281 enhances cardiac reprogramming by modulating cardiac and inflammatory gene expression. Genes Dev. *31*, 1770–1783.

STAR★METHODS

KEY RESOURCES TABLE

REAGENT or RESOURCE	SOURCE	IDENTIFIER
Antibodies		
Mouse monoclonal anti-Tnnt2	Thermo Fisher Scientific	Cat#MA5-12960; RRID: AB_11000742
Rabbit polyclonal anti-GFP	Thermo Fisher Scientific	Cat# A-11122; RRID: AB_221569
Alexa fluor 647 donkey anti-mouse IgG	Thermo Fisher Scientific	Cat# A-31571; RRID:AB_162542
Alexa fluor 488 goat anti-rabbit IgG	Thermo Fisher Scientific	Cat# A-11008; RRID:AB_143165
Alexa fluor 555 goat anti-mouse IgG	Thermo Fisher Scientific	Cat# A-28180; RRID:AB_2536164
Alexa fluor 488 donkey anti-rabbit IgG	Thermo Fisher Scientific	Cat# A-21206; RRID:AB_2535792
Goat polyclonal anti-Gata4	Santa Cruz Biotechnology	Cat# sc-1237; RRID: AB_2108747
Goat polyclonal anti-Tbx5	Santa Cruz Biotechnology	Cat# sc-17866; RRID:AB_2200827
Mouse monoclonal anti-Ty1	Diagenode	Cat# C15200054
Rabbit polyclonal anti-H3K27ac	Diagenode	Cat# C15410196; RRID:AB_2637079
Rabbit monoclonal anti-Mef2c	Cell Signaling	Cat# 5030; RRID:AB_10548759
Goat polyclonal anti-Hand2	R&D Systems	Cat# AF3876; RRID:AB_2295155
Mouse monoclonal anti-Gapdh	Merck Millipore	Cat# MAB374; RRID:AB_2107445
Rabbit polyclonal anti-mCherry	Abcam	Cat# ab167453; RRID:AB_2571870
Bacterial and Virus Strains		
One Shot™ TOP10 Chemically Competent E. coli	Thermo Fisher Scientific	C404010
One Shot™ Stbl3™ Chemically Competent E. coli	Thermo Fisher Scientific	C737303
Chemicals, Peptides, and Recombinant Proteins		
Erlotinib	Selleckchem	S1032
Ruxolitinib	Selleckchem	S1378
Gefitinib	Selleckchem	ZD1839
AZD1480	Selleckchem	S2162
B27 supplements	Invitrogen	17504-044
SureCoat	Cellutron	sc9035
Insulin, Transferrin, Selenium Solution	Invitrogen	41400045
MEM Non-Essential Amino Acids Solution	Invitrogen	11140050
MEM Vitamin Solution	Invitrogen	11120052
MEM Amino Acids Solution	Invitrogen	11130051
Matrigel	Corning	354248
4',6-diamidino-2-phenylindole	Thermo Fisher Scientific	D1306
Hoechst 33342, Trihydrochloride, Trihydrate	Thermo Fisher Scientific	H3570
Critical Commercial Assays		
ChIP-IT Express	Active Motif	53008
BLOCK-iT U6 RNAi Entry Vector Kit	Thermo Fisher Scientific	K494500
Deposited Data		
Raw and analyzed data	This paper	GEO: GSE112315, GEO: GSE112316, GEO: GSE112317
Experimental Models: Cell Lines		
Platinum-E (Plat-E) Retroviral Packaging Cell Line	Cell Biolabs	RV-101
HEK-293 Cell Line	ATCC	CRL-1573; RRID:CVCL_0045
Experimental Models: Organisms/Strains		
Mouse: αMHC-GFP	Song et al., 2012	N/A
Mouse: C57BL/6J	The Jackson Laboratory	N/A

(*Continued on next page*)

Continued

REAGENT or RESOURCE	SOURCE	IDENTIFIER
Oligonucleotides		
Primer: Mouse Myh6 Forward: 5′-GCC CAG TAC CTC CGA AAG TC-3′	This paper	N/A
Primer: Mouse Myh6 Reverse: 5′-GCC TTA ACA TAC TCC TTG TC-3′	This paper	N/A
Primer: Mouse Tnnt2 Forward: 5′-GTA GAG GAC ACC AAA CCC AAG-3′	This paper	N/A
Primer: Mouse Tnnt2 Reverse: 5′-GAG TCT GTA GCT CAT TCA GGT C-3′	This paper	N/A
Primer: Mouse Gapdh Forward: 5′-AGG TCG GTG TGA ACG GAT TTG-3′	This paper	N/A
Primer: Mouse Gapdh Reverse: 5′-TGT AGA CCA TGT AGT TGA GGT CA-3′	This paper	N/A
Jak2 shRNA sequence: 5′- GGTGGAATTCAGTGG TCAAGAcgaaTCTTGACCACTGAATTCCACC-3′	This paper	N/A
LacZ shRNA sequence: 5′- CTACACAAATCAGCG ATTTcgaaAAATCGCTGATTTGTGTAG-3′	This paper	N/A
Recombinant DNA		
pMXs-GW	Addgene	#18656; RRID:Addgene_18656
pMXs-puro	Cell Biolabs, Inc.	RTV-012
pMXs-Mef2c-3xTy1	This paper	N/A
pMXs-3xTy1-Hand2	This paper	N/A
pBabeX-Gata4	Song et al., 2012	N/A
pBabeX-Hand2	Song et al., 2012	N/A
pBabeX-Mef2c	Song et al., 2012	N/A
pBabeX-Tbx5	Song et al., 2012	N/A
Gja5 enhancer-Hsp68-LacZ	This paper	N/A
Tnni1 enhancer-Hsp68-LacZ	This paper	N/A
pMXs-puro-Gja5 enhancer-Hsp68-mCherry	This paper	N/A
pMXs-puro-Tnni1 enhancer-Hsp68-mCherry	This paper	N/A
pRS-Egfr shRNA	ORIGENE	TR509941
pMXs-Jak2 shRNA	This paper	N/A
Software and Algorithms		
FlowJo v10.5.3	FLOWJO, LCC	https://www.flowjo.com/
Cytoscape v3.6.0	Institute for Systems Biology	https://cytoscape.org/
R v3.4.1	The R Foundation	https://www.r-project.org/foundation/
MACS v2.1.0	Feng et al., 2012	http://liulab.dfci.harvard.edu/MACS/
GREAT	McLean et al., 2010	http://great.stanford.edu/public/html/
BEDTools v2.26.0	Quinlan and Hall, 2010	https://bedtools.readthedocs.io/en/latest/

CONTACT FOR REAGENT AND RESOURCE SHARING

Further information and requests for resources and reagents should be directed to and will be fulfilled by the Lead Contact, Eric Olson (eric.olson@utsouthwestern.edu).

EXPERIMENTAL MODEL AND SUBJECT DETAILS

Cell lines

Platinum-E (Plat-E) Retroviral Packaging Cell Lines (Cell Biolabs) were grown in DMEM supplemented with 10% fetal bovine serum (FBS), 1% penicillin/streptomycin, 10 μg/mL blasticidin (Thermo Fisher Scientific), and 1 μg/mL puromycin (Thermo Fisher Scientific). Plat-E cells under ten passages were used for retrovirus production. HEK-293 cells were grown in DMEM supplemented with 10% FBS and 1% penicillin/streptomycin, and were used for Western Blotting as described below.

Mice

All experiments involving animals were approved by the Institutional Animal Care and Use Committee at the University of Texas Southwestern Medical Center. All mice used in this study were housed at the Animal Resource Center at the University of Texas Southwestern Medical Center and bred inside a SPF facility with 12h light/dark cycles and monitored daily with no health problems reported. All animals were housed in groups of maximum five per cage with *ad libitum* access to food and water. αMHC-GFP mice were maintained on a mixed C57BL/6 background (Song et al., 2012).

METHOD DETAILS

Cell culture

MEFs from E13.5-14.5 C57BL/6 or αMHC-GFP mice were prepared as previously described (Nam et al., 2014) and cultured in fibroblast growth medium (DMEM containing 10% FBS and 1% penicillin/streptomycin) until experiments were performed. Adult mouse tail tip fibroblasts and cardiac fibroblasts from 4-6 weeks old C57BL/6 or αMHC-GFP were prepared as previously described and cultured in fibroblast growth medium until experiments were performed (Zhou et al., 2017). Mouse sex was not identified since fibroblasts used for each experiment were collected from a litter.

Retrovirus production and cardiac reprogramming

Generation of retroviral expression constructs encoding Gata4, Hand2, Mef2c, Tbx5, and Akt1 has been previously described (Song et al., 2012; Zhou et al., 2015). Retroviral construct for the expression of shRNA targeting Egfr was purchased from Origene. For generating the retroviral construct of shRNA targeting LacZ and Jak2, sequence 5′- CTACACAAATCAGCGATTTcgaaAAATCGCT GATTTGTGTAG-3′ and sequence 5′- GGTGGAATTCAGTGGTCAAGAcgaaTCTTGACCACTGAATTCCACC-3′ were cloned into an entry vector using BLOCK-iT U6 Entry Vector Kit (Thermo Scientific) and recombined into pMXs-GW vector by Gateway cloning. pMXs-GW was a gift from Dr. Shinya Yamanaka (Addgene plasmid # 18656) (Takahashi and Yamanaka, 2006). For some ChIP experiments, retroviral constructs that have a 3xTy1-epitope tag added to the N terminus of mouse Hand2 or the C terminus of mouse Mef2c were used. Retroviruses were produced using Platinum E cells, as described previously (Zhou et al., 2017). Briefly, retroviral constructs were transfected into Platinum E cells using FuGENE 6 transfection reagent. Twenty-four hours after transfection, wild-type or αMHC-GFP fibroblasts were seeded into culture dishes or plates that were precoated with SureCoat (Cellutron) or Matrigel (Corning). Forty-eight hours after transfection, the viral medium was filtered through a 0.45-μm filter and polybrene was added at a concentration of 8 μg/mL. Then fibroblasts were infected by replacing growth medium with the above viral mixture. The viral infection was serially repeated twice and twenty-four hours after the second infection, the viral medium was replaced with induction medium, composed of DMEM/199 (4:1), 10% FBS, 5% horse serum, 1% penicillin/streptomycin, 1% nonessential amino acids, 1% essential amino acids, 1% B-27, 1% insulin–selenium–transferrin, 1% vitamin mixture, and 1% sodium pyruvate (Invitrogen). Induction medium was replaced every two to three days until experiments were performed. Chemical compounds: 5 μM Erlotinib (Selleckchem, S1032); 5 μM Ruxolitinib (Selleckchem, S1378); 5 μM Gefitinib (Selleckchem, ZD1839); 2.5 μM AZD 1480 (Selleckchem, S2162) were freshly added to induction medium each time after medium change.

Quantitative mRNA measurement

Total RNA was extracted using TRIzol (Invitrogen) according to the vender's protocol. RNA was reverse-transcribed to cDNA using iScript Supermix (Bio-Rad). qPCR was performed using KAPA SYBR Fast (Kapa Biosystems) and gene expression was analyzed by the Ct method. Primers used were Fw 5′-GCC CAG TAC CTC CGA AAG TC-3′ and Rv 5′-GCC TTA ACA TAC TCC TTG TC-3′ for Myh6 and primers Fw 5′-GTA GAG GAC ACC AAA CCC AAG-3′ and Rv 5′- GAG TCT GTA GCT CAT TCA GGT C-3′ for Tnnt2. For input normalization, we used Gapdh Fw 5′-AGG TCG GTG TGA ACG GAT TTG-3′ and Rv 5′-TGT AGA CCA TGT AGT TGA GGT CA-3′. Measurements were recorded in triplicate.

Immunocytochemistry

Immunocytochemistry was performed as previously described (Zhou et al., 2015). Briefly, cells were fixed in 4% PFA for 15 min at room temperature and blocked with 5% goat serum. Fixed cells were then incubated on a rotator with mouse monoclonal anti-Tnnt2 antibody (1:500, Thermo Scientific, MA5-12960), rabbit anti-GFP antibody (1:500, Thermo Scientific, A-11122), and rabbit anti-mCherry antibody (1:500, Abcam, ab167453) in 5% goat serum for 1 h at room temperature or 4 °C overnight. After three washes with PBS, cells were incubated with appropriate Alexa fluorogenic secondary antibodies (1:500, Invitrogen) at room temperature for 1 hr. Image acquisition and analysis was done on a BZ-X710 (Keyence). For quantification, cells were manually quantified and averaged to yield an individual replicate in four randomly selected low-power fields of view from each well in three independent experiments.

Western blot analyses

HEK-293 cells were transfected with plasmids using FuGENE6 and cell lysates were analyzed after 48 hours of transfection. Western blot analyses were performed as previously described (Song et al., 2012). Briefly, cell lysates were prepared using RIPA buffer with complete protease inhibitor cocktail tablets (Roche). Lysates were boiled with 4x Laemmli buffer for 5 min at 95°C. Antibodies used were anti-Mef2c antibody (1:1000, Cell Signaling, 5030), anti-Hand2 antibody (1:200, R&D Systems, AF3876), anti-Ty1 antibody (1:1000, Diagenode, C15200054), and anti-Gapdh antibody (1:1000, Merck Millipore, MAB374).

Flow cytometry

Flow cytometry was performed as previously described (Zhou et al., 2017). Briefly, cells were trypsinized, harvested, and suspended into single cells. Then cells were fixed and permeabilized using BD Cytofix/Cytoperm (BD Biosciences). Antibodies used were mouse monoclonal anti-Tnnt2 antibody (1:200, Thermo Scientific, MA5-12960), rabbit anti-GFP antibody (1:200, Thermo Scientific, A-11122), donkey anti-mouse Alexa fluor 647 (1:200, Invitrogen, A-31571) and goat anti-rabbit Alexa fluor 488 (1:200, Invitrogen, A-11008). Cells were analyzed using FACSCalibur (BD Biosciences) and FlowJo software (FLOWJO, LCC).

Beating cell analysis and calcium assay

Beating cell analyses were performed as previously described on Matrigel coated dish (Corning, 354248) (Zhou et al., 2015). Beating cells were manually counted in eight randomly selected high-power fields per well in at least three independent experiments. Calcium assay was performed as previously described on Matrigel coated dishes with some modification (Zhou et al., 2015). Fluo-4 NW Calcium Assay Kit (Thermo Scientific, F36206) was used according to the manufacturer's protocol and Ca^{2+} flux was measured on fibroblasts 10 days after retroviral treatment. Briefly, after replacing culture medium with the dye loading solution, plates were incubated at 37°C for 30 minutes, then at room temperature for an additional 30 minutes before measurement. Ca^{2+} flux positive cells were manually counted in ten randomly selected high-power fields per well in three independent experiments.

In vitro and *in vivo* transgenic reporter assays

Enhancer names tested in this study are the unique identifiers used in the VISTA Enhancer Browser (https://enhancer.lbl.gov/) (Visel et al., 2007). Putative *Gja5* and *Tnni1* enhancers were cloned into an hsp68-lacZ expression vector and LacZ transgenic mouse assays were conducted as previously described (Kothary et al., 1989; Liu et al., 2007; Visel et al., 2007). Embryos were collected at indicated stages and stained for β-galactosidase activity, and mice carrying LacZ transgenes were identified by PCR analysis. For *in vitro* reporter assay, LacZ coding sequences from *Tnni1*-E- and *Gja5*-E-Hsp68-LacZ plasmids were removed with KasI and MfeI digestion, and replaced by mCherry coding sequences using Infusion cloning. Then *Tnni1*-E- and *Gja5*-E-Hsp68-mCherry expression cassettes were PCR amplified with a XhoI site on enhancer end (5′) and a BamHI site on mCherry end (3′) and cloned into BamHI and XhoI linearized pMXs-Puro plasmid by Infusion cloning. The *Tnni1*-E- or *Gja5*-E-Hsp68-mCherry construct was retrovirally delivered to MEFs together with reprogramming factors and mCherry expression was investigated in iCLMs. Genomic coordinates of all enhancers are listed in Table S5.

ChIP-seq sample preparation

For ChIP-seq sample preparation, MEFs two or seven days after retroviral transduction were crosslinked with 1% formaldehyde in PBS for 30 min and neutralized by the addition of glycine to a final concentration of 0.125M for 5 min. MEFs were then harvested and washed with cold PBS for ChIP. For mouse heart sample preparation, ChIP was performed as previously described (Huang et al., 2016; Xu et al., 2012), or by using ChIP-IT Express ChIP kits (Active Motif) following the vender's protocol. In brief, cell lysates were sonicated (ten cycles of 30 s on/off) to shear DNA using a Bioruptor Pico sonicator (Diagenode, B01060010). Then, chromatin was incubated with indicated antibodies overnight at 4 °C. Pre-washed rinsed Dynabeads (protein G) were then added to the antibody-treated chromatin, and immunoprecipitation was performed on a rotator for 3 hours at 4 °C. The following antibodies were used for ChIP experiments: anti-Gata4 antibody (Santa Cruz Biotechnology, sc-1237), anti-Tbx5 antibody (Santa Cruz Biotechnology, sc-17866), anti-Ty1 antibody (Diagenode, C15200054), and anti-H3K27ac antibody (Diagenode, C15410196). ChIP-seq libraries were generated using KAPA Hyper Prep Kit following the manufacturer's protocol (Kapa Biosystems), and single-end sequenced on the Illumina NextSeq500 system using the 75bp high output sequencing kit. Subsequent massive parallel sequencing was performed at the University of Texas Southwestern Genomics and Microarray Core Facility or the Sequencing Core Facility in Children's Medical Center Research Institute at University of Texas Southwestern Medical Center.

RNA-seq sample preparation

For RNA-seq sample preparation, total RNA was extracted from MEFs two or seven days after retroviral transduction, using TRIzol (Invitrogen) according to the vender's protocol. Illumina RNA-seq was performed by the University of Texas Southwestern Microarray Core Facility.

QUANTIFICATION AND STATISTICAL ANALYSIS

ChIP-seq analysis

The raw reads were aligned to the mouse reference genome (GRCh38/mm10) using default parameters in BWA version 0.7.12 (Li and Durbin, 2009). The aligned reads were subsequently filtered for quality and uniquely mappable reads were retained for further analysis using Samtools version 1.3 (Li et al., 2009) and Sambamba version 0.6.6 (Tarasov et al., 2015). Library complexity was measured using BEDTools version 2.26.0 (Quinlan and Hall, 2010) and met ENCODE data quality standards (Landt et al., 2012). Relaxed peaks were called using MACS version 2.1.0 (Feng et al., 2012) with a p value of $1x10^{-2}$ for H3K27ac and SPP version 1.4 (Kharchenko et al., 2008) with an IDR = 0.01 for each replicate and pseudoreplicate. For H3K27ac, peak calls that were observed in either all replicates or both pseudoreplicates were used for subsequent analysis. For ENCODE data, raw data were downloaded from the Data Coordination Center of the ENCODE project (https://www.encodeproject.org/). For annotating active enhancers, we used the peaks of

H3K27ac and excluded peaks located in promoter regions (±2kb from TSS). GREAT (McLean et al., 2010) was used for GO, Signaling pathway, and MGI expression analysis. To generate the heatmap and profiles of ChIP-seq intensities, we used deepTools version 2.5.0 (Ramírez et al., 2016) to generate read abundance from all ChIP-seq datasets around peak center (±5.0kb/ 2.5 kb/ 2.0 kb), using computeMatrix. These matrices were then used to generate heatmaps or profiles, using plotHeatmap or plotProfile, respectively. To identify enriched motifs within each type of enhancer, we performed motif enrichment analysis using HOMER version 4.9 as previously described (Heinz et al., 2010, 2015). Significance analysis of global enhancer activity was calculated using the hypergeometric distribution given the number of enhancers to nearest neighboring gene overlapped to regulated genes for each condition under comparison and the total number of genes in the genome.

RNA-seq analysis

Following sequencing as described above, reads with Phred quality scores less than 20 and less than 35 bp after trimming were removed from further analysis using trimgalore version 0.4.1. Quality-filtered reads were then aligned to the mouse reference genome GRCm38 (mm10) using the HISAT2 (v 2.0.1) (Pertea et al., 2016) aligner with default settings and marked duplicates using Sambamba version 0.6.6 (Tarasov et al., 2015). Aligned reads were quantified using featurecount (v1.4.6) (Liao et al., 2014) per gene ID against Gencode version 10 (Mudge and Harrow, 2015). Differential gene expression analysis was done using the R package DEseq2 (v 1.6.3). Cutoff values of absolute fold change greater than 1.0 and FDR $\leq$ 0.01 were then used to select for differentially expressed genes between sample group comparisons. Normalized gene count values were averaged within groups for heatmap generation and clustered using the R package clusterProfiler (v3.6.0) (Yu et al., 2012). GO enrichment and pathway analysis was performed using PANTHER to determine molecular and biological functional categories (Mi et al., 2017). Volcano plots were generated using the R package ggplot2. DAVID (v6.8) gene functional annotation and classification tool (Huang et al., 2009a, 2009b) was used to annotate the list of differentially expressed genes with respective Gene Ontology terms and perform GO enrichment analysis for biological function category. The enrichGO function in clusterProfiler (v3.6.0) (Yu et al., 2012) was used to perform GO enrichment analysis for each cluster. Gene Ontology groups were selected for significance using a p value cutoff of 0.01.

Gene regulatory network analysis

Each ChIP-seq TF peak was annotated to its nearest gene using HOMER (version 4.9). These genes were overlapped with the RNA-seq data and clustered based on their differential gene expression. The TF to gene interaction matrix was visualized using Cytoscape (v3.6.0). Genes which appeared in GMT or GHMT TF peaks annotation, but did not show up in the GHMT or AGHMT TF peaks annotation, respectively, were excluded from the analysis. The set of nearest neighboring genes for each active enhancer was determined for each cell line group.

Statistical analysis

Statistical analyses were performed using GraphPad Prism 7 (GraphPad Software, Inc.) and statistical significance ($p < 0.05$) was determined using the Student's t test. All data are presented as mean ± SD (error bars).

DATA AND SOFTWARE AVAILABILITY

All ChIP-seq data can be accessed at Gene Expression Omnibus (GEO) Series: GEO: GSE112315. All RNA-seq data can be accessed at GEO Series: GEO: GSE112316. All datasets used in this paper have been deposited in the GEO with accession number: GEO: GSE112317.

Cell Stem Cell, Volume *25*

Supplemental Information

Cardiac Reprogramming Factors Synergistically Activate Genome-wide Cardiogenic Stage-Specific Enhancers

Hisayuki Hashimoto, Zhaoning Wang, Glynnis A. Garry, Venkat S. Malladi, Giovanni A. Botten, Wenduo Ye, Huanyu Zhou, Marco Osterwalder, Diane E. Dickel, Axel Visel, Ning Liu, Rhonda Bassel-Duby, and Eric N. Olson

Supplemental Information

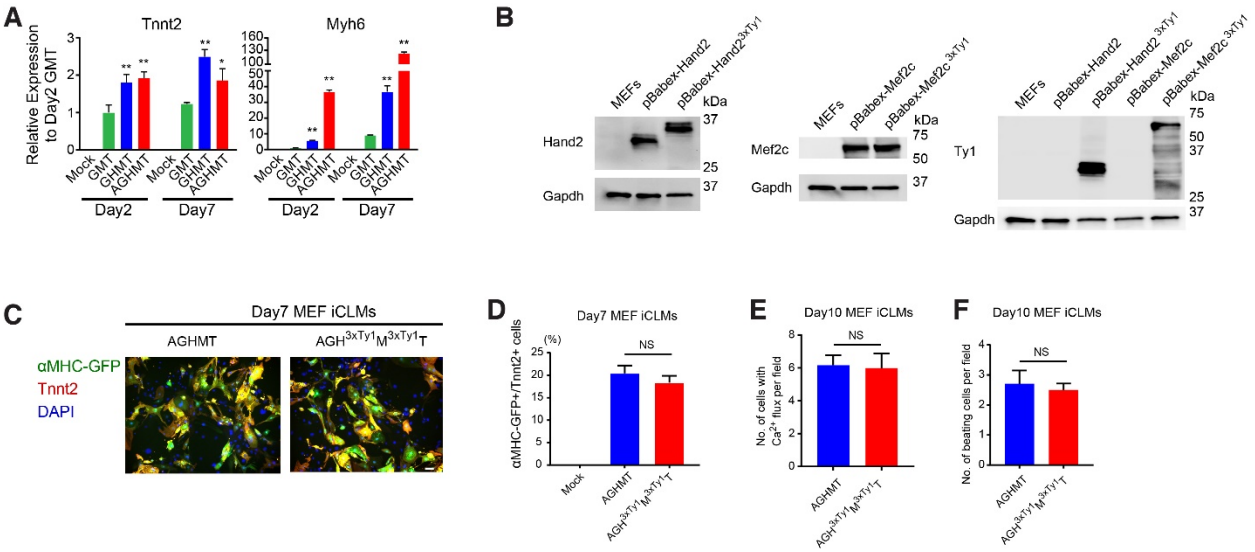

Figure S1, related to Figure 1. Cardiac Reprogramming by Tagged Reprogramming Factors.

(A) Transcript levels of Tnnt2 and Myh6 were increased 2 days after induction by adding Hand2 and Akt1 to GMT in MEFs. Transcript levels are normalized to Gapdh (n = 3, independent experiments). (* P< 0.05 vs. GMT, ** P< 0.01 vs. GMT). Data represented as mean ± SD.

(B) Western blot of 3xTy1 tagged Hand2 and Mef2c expressed in HEK293 cells.

(C) Representative immunocytochemistry images of day 7 αMHC-GFP transgenic MEFs treated with AGHMT or AGH^{3xTy1}M^{3xTy1}T. Cells were fixed and stained for αMHC-GFP (green), Tnnt2 (red), and DAPI (blue) 7 days after infection. Bars, 100 um.

(D) Quantification by flow cytometry of αMHC-GFP+ and Tnnt2+ iCLMs 7 days after infection with AGHMT or AGH^{3xTy1}M^{3xTy1}T (n = 3, independent experiments). Data represented as mean ± SD.

(E) Quantification of Ca^{2+} flux-positive MEFs after 10 days of reprogramming using Fluo-4 NW dye (n = 3, independent experiments). Data represented as mean ± SD.

(F) Quantification of spontaneous beating iCLMs 10 days after reprogramming (n = 3, independent experiments). Data represented as mean ± SD.

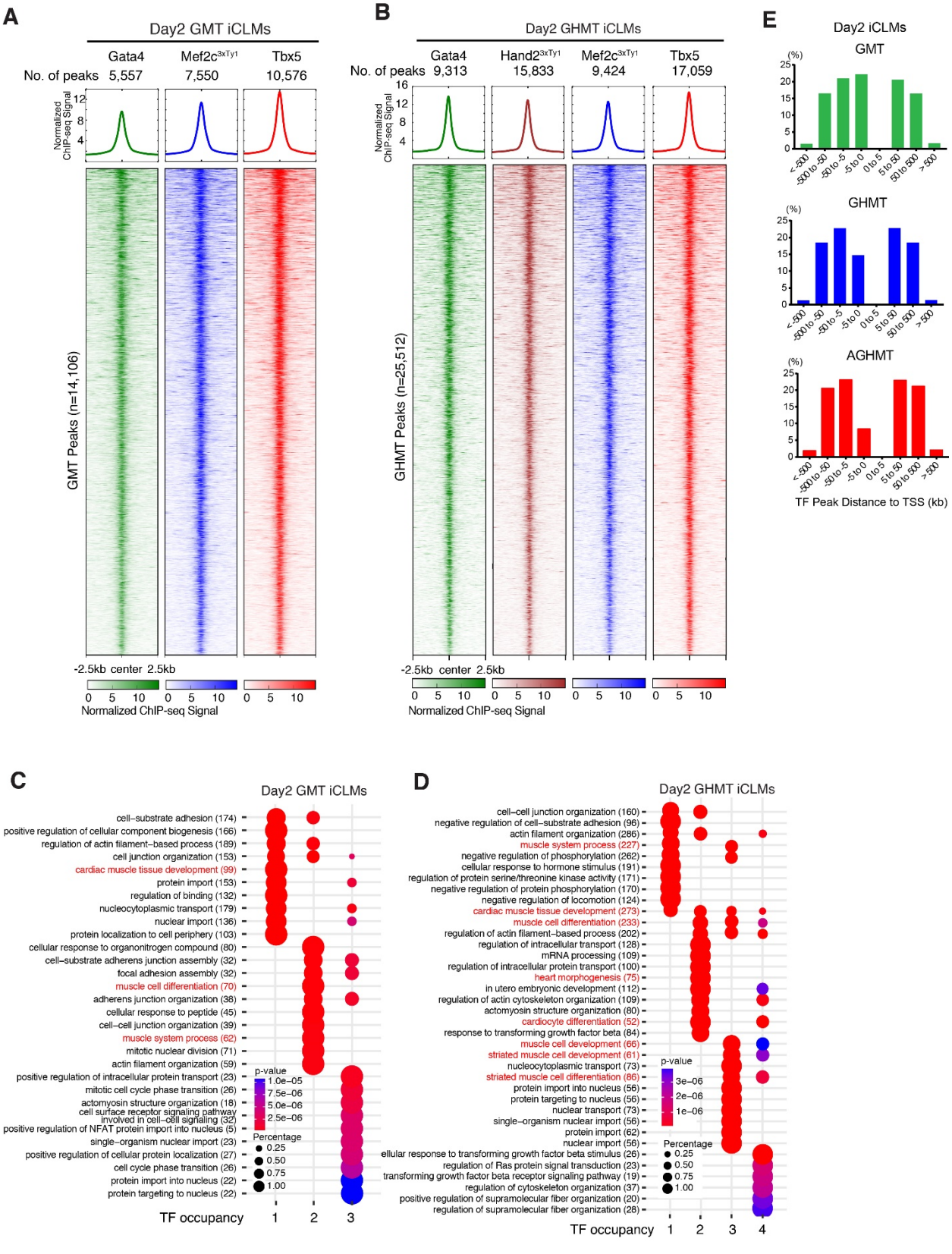
A
Day2 GMT iCLMs
Gata4
Mef2c3xTy1
Tbx5
No. of peaks 5,557
7,550
10,576
Normalized ChIP-seq Signal
GMT Peaks (n=14,106)
-2.5kb center 2.5kb
Normalized ChIP-seq Signal
B
Day2 GHMT iCLMs
Gata4
Hand23xTy1
Mef2c3xTy1
Tbx5
No. of peaks 9,313
15,833
9,424
17,059
GHMT Peaks (n=25,512)
-2.5kb center 2.5kb
Normalized ChIP-seq Signal
E
Day2 iCLMs
GMT
GHMT
AGHMT
(%)
TF Peak Distance to TSS (kb)
C
Day2 GMT iCLMs
cell−substrate adhesion (174)
positive regulation of cellular component biogenesis (166)
regulation of actin filament−based process (189)
cell junction organization (153)
cardiac muscle tissue development (99)
protein import (153)
regulation of binding (132)
nucleocytoplasmic transport (179)
nuclear import (136)
protein localization to cell periphery (103)
cellular response to organonitrogen compound (80)
cell−substrate adherens junction assembly (32)
focal adhesion assembly (32)
muscle cell differentiation (70)
adherens junction organization (38)
cellular response to peptide (45)
cell−cell junction organization (39)
muscle system process (62)
mitotic nuclear division (71)
actin filament organization (59)
positive regulation of intracellular protein transport (23)
mitotic cell cycle phase transition (26)
actomyosin structure organization (18)
cell surface receptor signaling pathway involved in cell−cell signaling (32)
positive regulation of NFAT protein import into nucleus (5)
single−organism nuclear import (23)
positive regulation of cellular protein localization (27)
cell cycle phase transition (26)
protein import into nucleus (22)
protein targeting to nucleus (22)
p-value
Percentage
TF occupancy
D
Day2 GHMT iCLMs
cell−cell junction organization (160)
negative regulation of cell−substrate adhesion (96)
actin filament organization (286)
muscle system process (227)
negative regulation of phosphorylation (262)
cellular response to hormone stimulus (191)
regulation of protein serine/threonine kinase activity (171)
negative regulation of protein phosphorylation (170)
negative regulation of locomotion (124)
cardiac muscle tissue development (273)
muscle cell differentiation (233)
regulation of actin filament−based process (202)
regulation of intracellular transport (128)
mRNA processing (109)
regulation of intracellular protein transport (100)
heart morphogenesis (75)
in utero embryonic development (112)
regulation of actin cytoskeleton organization (109)
actomyosin structure organization (80)
cardiocyte differentiation (52)
response to transforming growth factor beta (84)
muscle cell development (66)
striated muscle cell development (61)
nucleocytoplasmic transport (73)
striated muscle cell differentiation (86)
protein import into nucleus (58)
protein targeting to nucleus (56)
nuclear transport (73)
single−organism nuclear import (56)
protein import (62)
nuclear import (56)
cellular response to transforming growth factor beta stimulus (26)
regulation of Ras protein signal transduction (23)
transforming growth factor beta receptor signaling pathway (19)
regulation of cytoskeleton organization (37)
positive regulation of supramolecular fiber organization (20)
regulation of supramolecular fiber organization (28)
p-value
Percentage
TF occupancy

Figure S2, related to Figure 1. Genome-wide Co-occupancy of Reprogramming Factors in GMT and GHMT iCLMs.

(A,B) ChIP-seq data for Gata4, Mef2c, and Tbx5 reveals co-occupancy at 14,106 genomic binding sites 2 days following GMT-mediated reprograming of MEFs (A). ChIP-seq data for Gata4, Mef2c, Hand2, and Tbx5 reveals co-occupancy at 25,512 genomic binding sites 2 days following GHMT-mediated reprograming of MEFs (B). Normalized ChIP-seq binding profiles for TF in each cluster are shown.

(C,D) Each TF peak in GMT (C) or GHMT (D) MEF iCLMs was annotated to the nearest neighboring gene. GO enrichment analysis for biological process was performed with DAVID (v6.8). clusterProfiler (v3.6.0) was used to visualize GO term enrichment from different groups based on the number of occupying TFs. Terms related to heart or muscle are highlighted in red.

(E) Percentage of TF peaks in GMT, GHMT, and AGHMT iCLMs categorized by the distance to TSS.

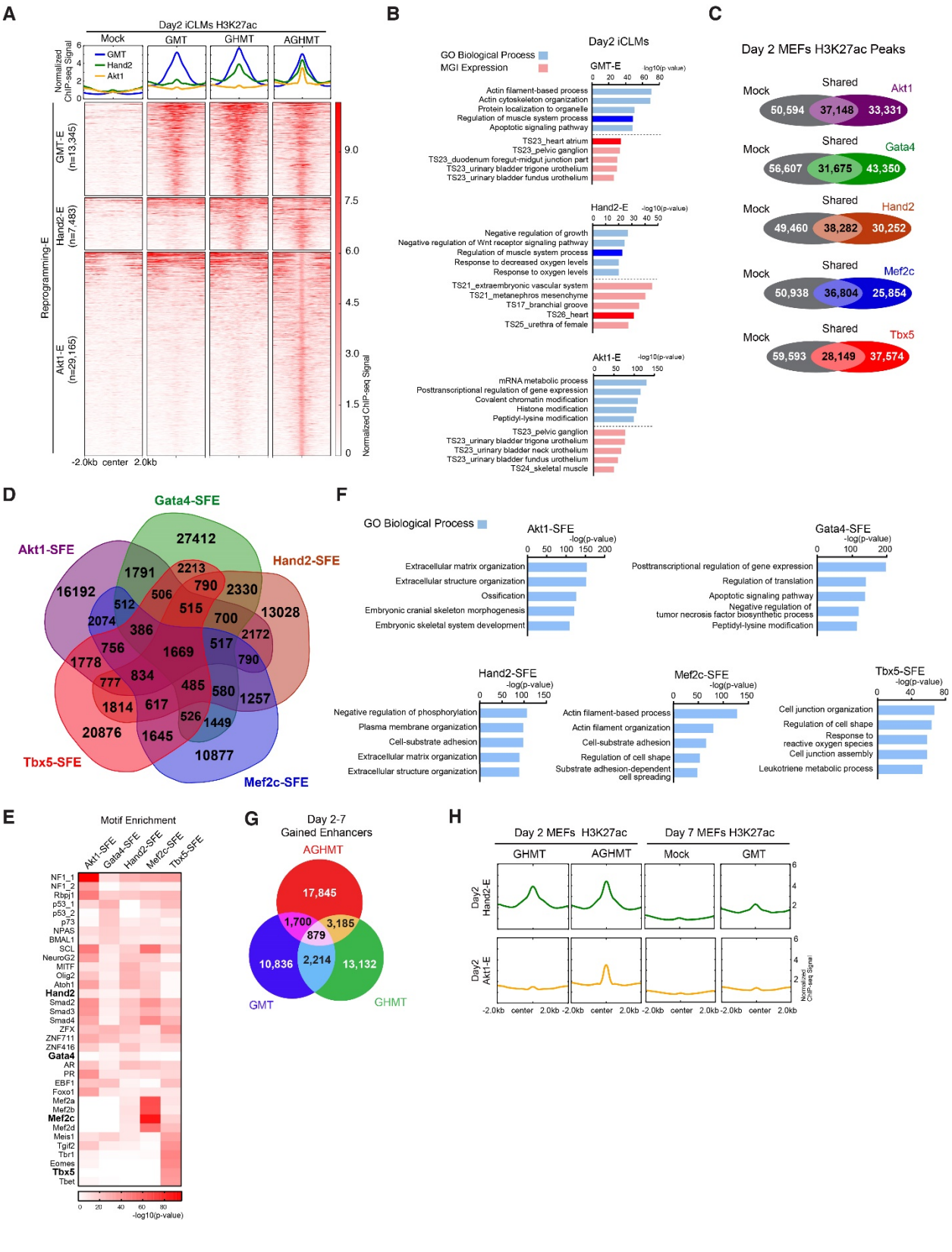
A
Day2 iCLMs H3K27ac
Mock
GMT
GHMT
AGHMT
Normalized ChIP-seq Signal
GMT
Hand2
Akt1
GMT-E (n=13,345)
Hand2-E (n=7,483)
Akt1-E (n=29,165)
Reprogramming-E
-2.0kb center 2.0kb
Normalized ChIP-seq Signal
B
Day2 iCLMs
GO Biological Process
MGI Expression
GMT-E
-log10(p-value)
Actin filament-based process
Actin cytoskeleton organization
Protein localization to organelle
Regulation of muscle system process
Apoptotic signaling pathway
TS23_heart atrium
TS23_pelvic ganglion
TS23_duodenum foregut-midgut junction part
TS23_urinary bladder trigone urothelium
TS23_urinary bladder fundus urothelium
Hand2-E
Negative regulation of growth
Negative regulation of Wnt receptor signaling pathway
Regulation of muscle system process
Response to decreased oxygen levels
Response to oxygen levels
TS21_extraembryonic vascular system
TS21_metanephros mesenchyme
TS17_branchial groove
TS26_heart
TS25_urethra of female
Akt1-E
mRNA metabolic process
Posttranscriptional regulation of gene expression
Covalent chromatin modification
Histone modification
Peptidyl-lysine modification
TS23_pelvic ganglion
TS23_urinary bladder trigone urothelium
TS23_urinary bladder neck urothelium
TS23_urinary bladder fundus urothelium
TS24_skeletal muscle
C
Day 2 MEFs H3K27ac Peaks
Mock
Shared
Akt1
50,594
37,148
33,331
Gata4
56,607
31,675
43,350
Hand2
49,460
38,282
30,252
Mef2c
50,938
36,804
25,854
Tbx5
59,593
28,149
37,574
D
Gata4-SFE
Akt1-SFE
Hand2-SFE
Tbx5-SFE
Mef2c-SFE
27412
16192
1791
2213
790
2330
13028
512
506
515
700
2074
386
2172
756
1669
517
790
1778
834
777
485
580
1257
1814
617
526
1449
20876
1645
10877
F
GO Biological Process
Akt1-SFE
-log(p-value)
Extracellular matrix organization
Extracellular structure organization
Ossification
Embryonic cranial skeleton morphogenesis
Embryonic skeletal system development
Gata4-SFE
Posttranscriptional regulation of gene expression
Regulation of translation
Apoptotic signaling pathway
Negative regulation of tumor necrosis factor biosynthetic process
Peptidyl-lysine modification
Hand2-SFE
Negative regulation of phosphorylation
Plasma membrane organization
Cell-substrate adhesion
Extracellular matrix organization
Extracellular structure organization
Mef2c-SFE
Actin filament-based process
Actin filament organization
Cell-substrate adhesion
Regulation of cell shape
Substrate adhesion-dependent cell spreading
Tbx5-SFE
Cell junction organization
Regulation of cell shape
Response to reactive oxygen species
Cell junction assembly
Leukotriene metabolic process
E
Motif Enrichment
Akt1-SFE
Gata4-SFE
Hand2-SFE
Mef2c-SFE
Tbx5-SFE
NF1_1
NF1_2
Rbpj1
p53_1
p53_2
p73
NPAS
BMAL1
SCL
NeuroG2
MITF
Olig2
Atoh1
Hand2
Smad2
Smad3
Smad4
ZFX
ZNF711
ZNF416
Gata4
AR
PR
EBF1
Foxo1
Mef2a
Mef2b
Mef2c
Mef2d
Meis1
Tgif2
Tbr1
Eomes
Tbx5
Tbet
-log10(p-value)
G
Day 2-7
Gained Enhancers
AGHMT
17,845
1,700
3,185
879
10,836
2,214
13,132
GMT
GHMT
H
Day 2 MEFs H3K27ac
Day 7 MEFs H3K27ac
GHMT
AGHMT
Mock
GMT
Day2 Hand2-E
Day2 Akt1-E
-2.0kb center 2.0kb
Normalized ChIP-seq Signal

Figure S3, related to Figure 2. Reprogramming Enhancer Activation Requires Cooperative Actions of Reprogramming Factors.

(A) Heatmap of H3K27ac ChIP-seq signals in Reprogramming-E peaks for day 2 Mock-infected MEFs, GMT-, GHMT-, or AGHMT-iCLMs using a 4kb-window. H3K27ac ChIP-seq signals in the Reprogramming-E peaks from (Figure 2A) were clustered into three groups depending on their response to GMT (GMT-E), GHMT (Hand2-E), and AGHMT (Akt1-E). Normalized ChIP-seq binding profiles for H3K27ac in each cluster are shown.

(B) H3K27ac enhancer peaks of day 2 reprogramming enhancers were functionally annotated using GREAT. Five of the most overrepresented terms belonging to the GO Biological Process (blue) and MGI Expression (red) in each enhancer cluster are shown. Terms related to heart or muscle are highlighted in dark colors.

(C) Venn diagrams showing the number of overlapping H3K27ac enhancer peaks between Mock and each single factor overexpressing MEFs.

(D) Venn diagram showing the number of overlapping H3K27ac peaks among each SFE region.

(E) Heatmap of known motifs enriched in each SFE region. Reprogramming TFs are in bold.

(F) H3K27ac peaks of each single factor overexpressing MEFs were functionally annotated using GREAT. Five of the most overrepresented terms belonging to the GO Biological Process are shown.

(G) Venn diagrams showing the number of overlapping H3K27ac peaks of gained enhancers between day 2 and 7 in GMT, GHMT, and AGHMT iCLMs.

(H) Normalized ChIP-seq binding profiles for H3K27ac in day 2 GHMT and AGHMT iCLMs and day 7 Mock and GMT iCLMs at day 2 Hand2-E and Akt1-E regions from (A).

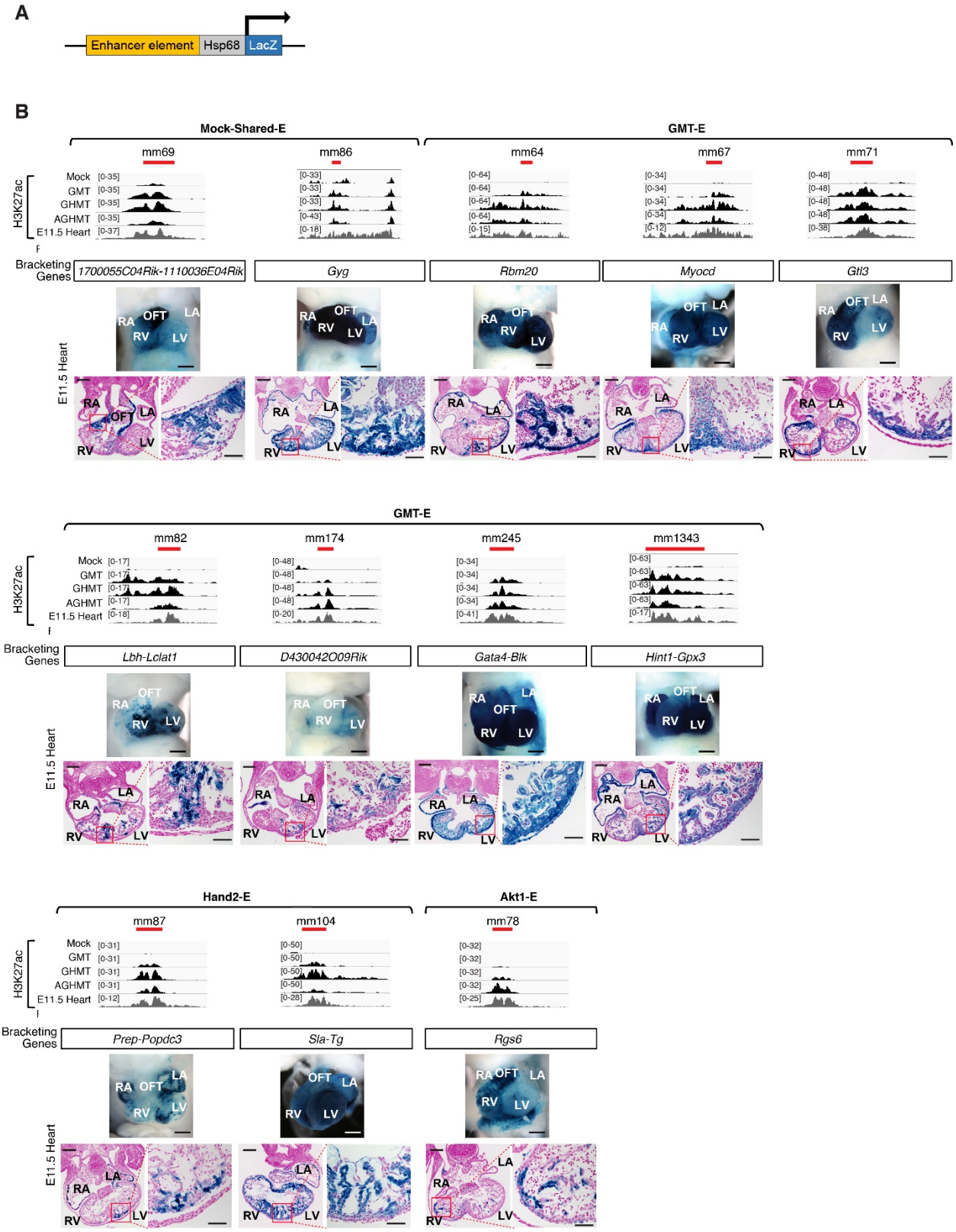
A
Enhancer element
Hsp68
LacZ
B
Mock-Shared-E
GMT-E
mm69
mm86
mm64
mm67
mm71
H3K27ac
Mock
GMT
GHMT
AGHMT
E11.5 Heart
Bracketing Genes
1700055C04Rik-1110036E04Rik
Gyg
Rbm20
Myocd
Gtl3
E11.5 Heart
RA
OFT
LA
RV
LV
GMT-E
mm82
mm174
mm245
mm1343
Lbh-Lclat1
D430042O09Rik
Gata4-Blk
Hint1-Gpx3
Hand2-E
Akt1-E
mm87
mm104
mm78
Prep-Popdc3
Sla-Tg
Rgs6

Figure S4, related to Figure 4. iCLM Enhancers Display Specific Expression Patterns in the Developing Heart.

(A) Schematic of Hsp68-LacZ construct for transgenic enhancer reporter assay.

(B) Cardiac subregional specificities of additional iCLM enhancers as shown in Figure 4B. (Black scale bars: 500μm for whole mount heart, 200μm and 50μm for low and high magnification histology sections, respectively)

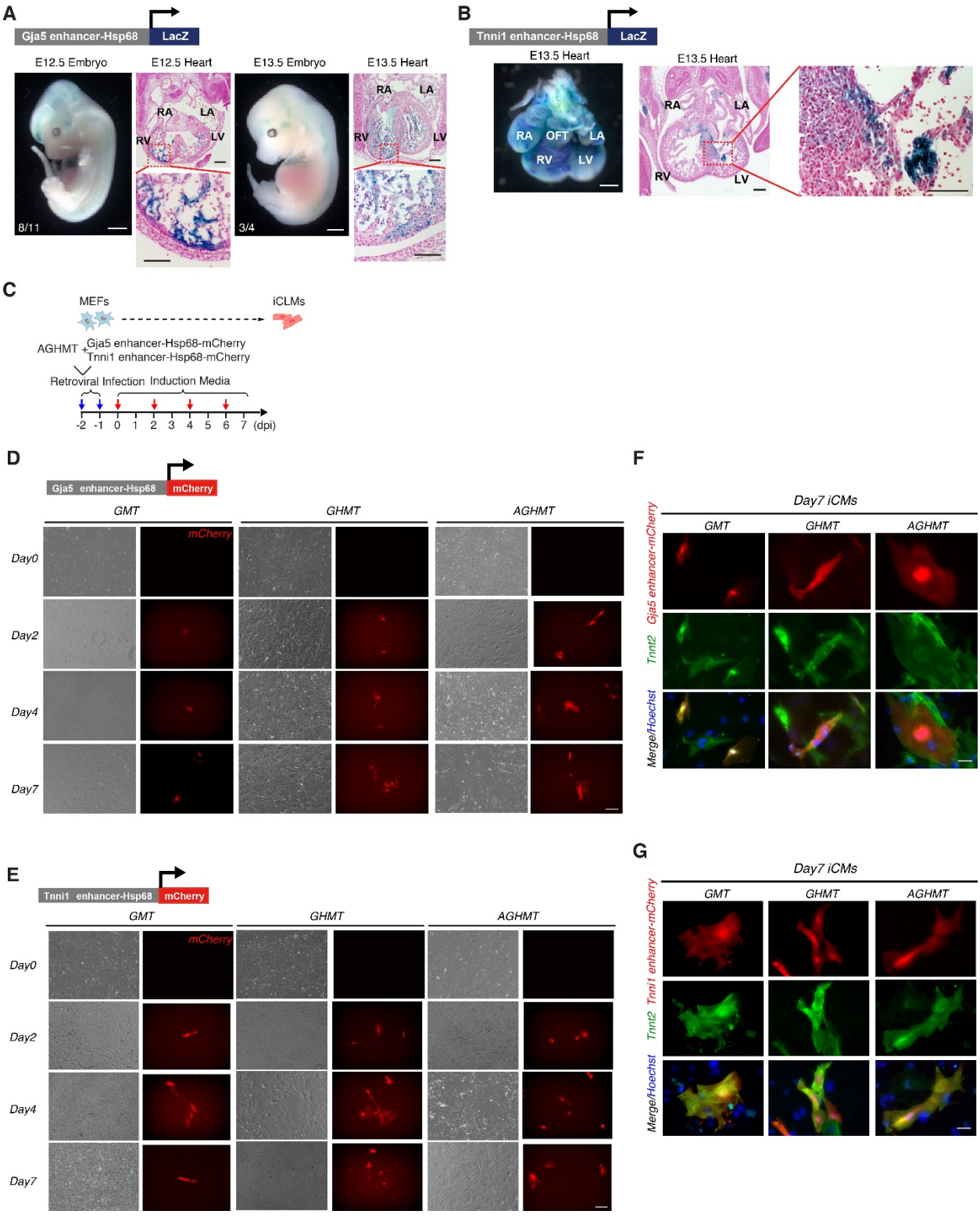
A
Gja5 enhancer-Hsp68
LacZ
E12.5 Embryo
E12.5 Heart
E13.5 Embryo
E13.5 Heart
RA
LA
RV
LV
8/11
3/4
B
Tnni1 enhancer-Hsp68
LacZ
E13.5 Heart
E13.5 Heart
RA
OFT
LA
RV
LV
C
MEFs
iCLMs
AGHMT +
Gja5 enhancer-Hsp68-mCherry
Tnni1 enhancer-Hsp68-mCherry
Retroviral Infection
Induction Media
-2 -1 0 1 2 3 4 5 6 7 (dpi)
D
Gja5 enhancer-Hsp68
mCherry
GMT
GHMT
AGHMT
Day0
Day2
Day4
Day7
F
Day7 iCMs
GMT
GHMT
AGHMT
Gja5 enhancer-mCherry
Tnnt2
Merge/Hoechst
E
Tnni1 enhancer-Hsp68
mCherry
G
Day7 iCMs
Tnni1 enhancer-mCherry

Figure S5, related to Figure 4. Putative *Gja5* and *Tnni1* Enhancer Activity at Different Stages of Embryonic Development and Reprogramming.

(A) Gross images of Gja5-E-Hsp68-LacZ transgenic whole embryos stained with β–galactosidase at E12.5 and E13.5. Section of E12.5 and E13.5 Gja5-E-Hsp68-LacZ transgenic heart counter-stained with Nuclear Fast Red showing expression of LacZ in the myocardium. Numbers indicate embryos with cardiac expression over the total LacZ+ genotyped embryos. (White scale bars: 1mm, Black scale bars: 200μm and 50μm for low and high magnification histology sections, respectively).

(B) Representative image of Tnni1-E-Hsp68-LacZ E13.5 transgenic heart stained with β-galactosidase showing LacZ expression in the heart (White scale bar: 500μm). Section of Tnni1-E-Hsp68-LacZ E13.5 transgenic heart stained with Nuclear Fast Red showing LacZ expression in the myocardium (Black scale bars: 200μm and 50μm for low and high magnification histology sections, respectively).

(C) Strategy for testing enhancer activity during direct cardiac reprogramming in MEFs. Gja5-E-Hsp68-mCherry or Tnni1-E-Hsp68-mCherry was retrovirally delivered to MEFs along with the reprogramming factors. (dpi, days post induction)

(D,E) Representative live cell images of day 0, 2, 4 and 7 Gja5-E-Hsp68-mCherry (D) or Tnni1-E-Hsp68-mCherry (E) iCLMs in different reprogramming cocktails showing mCherry expression. (Bars, 200μm).

(F,G) Representative immunocytochemistry images of GMT, GHMT and AGHMT iCLMs expressing mCherry under Gja5-E (F) or Tnni1-E (G) activity. Cells were fixed and stained for Tnnt2 (green), mCherry (red), and Hoechst (blue) 7 days after infection. (Bars, 50μm).

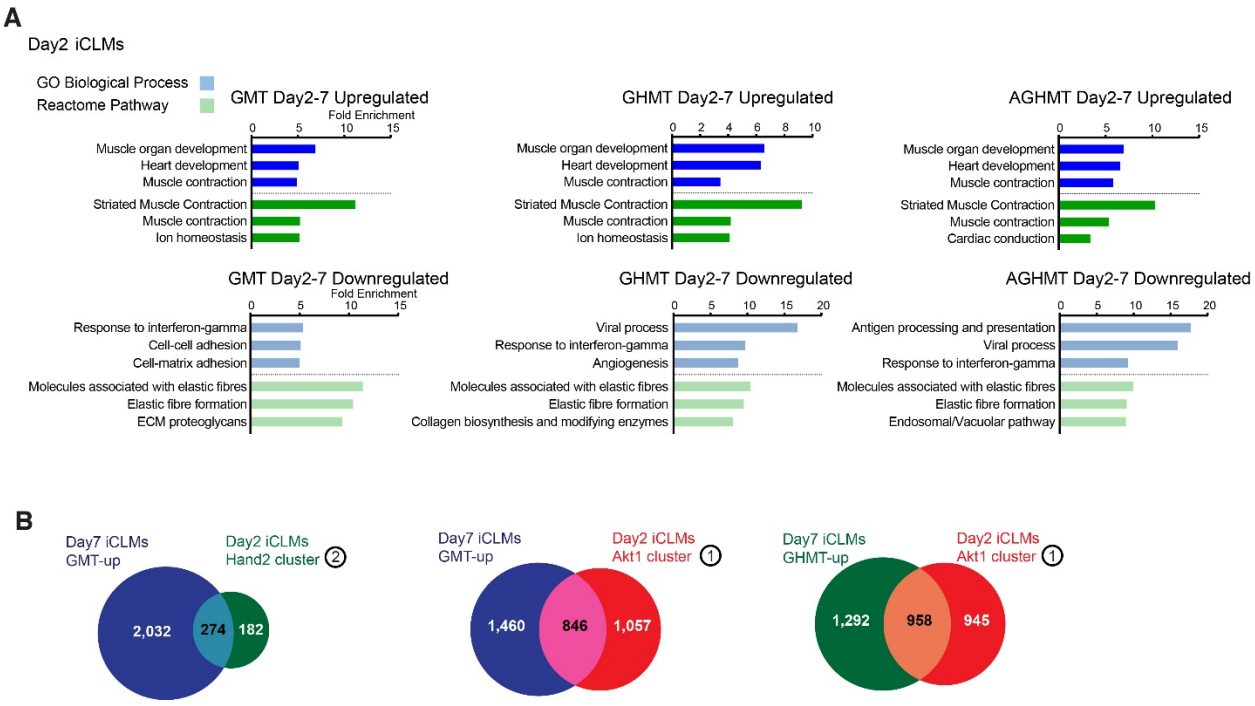

Figure S6, related to Figure 5. Time Dependent Activation of Cardiac Genes during Cardiac Reprogramming.

(A) Functional annotation of gene sets changing between day 2 and 7 iCLMs was performed by PANTHER and the three most overrepresented GO Biological Process (blue) and Reactome Pathway (green) terms are shown. Gene sets upregulated show high enrichment of terms related to heart or muscle development and contraction, which are highlighted in dark colors.

(B) Venn diagrams showing the number of overlapping genes between the upregulated genes in day 7 GMT and GHMT iCLMs with day 2 iCLM Hand2 and Akt1 cluster from (Figure 5E).

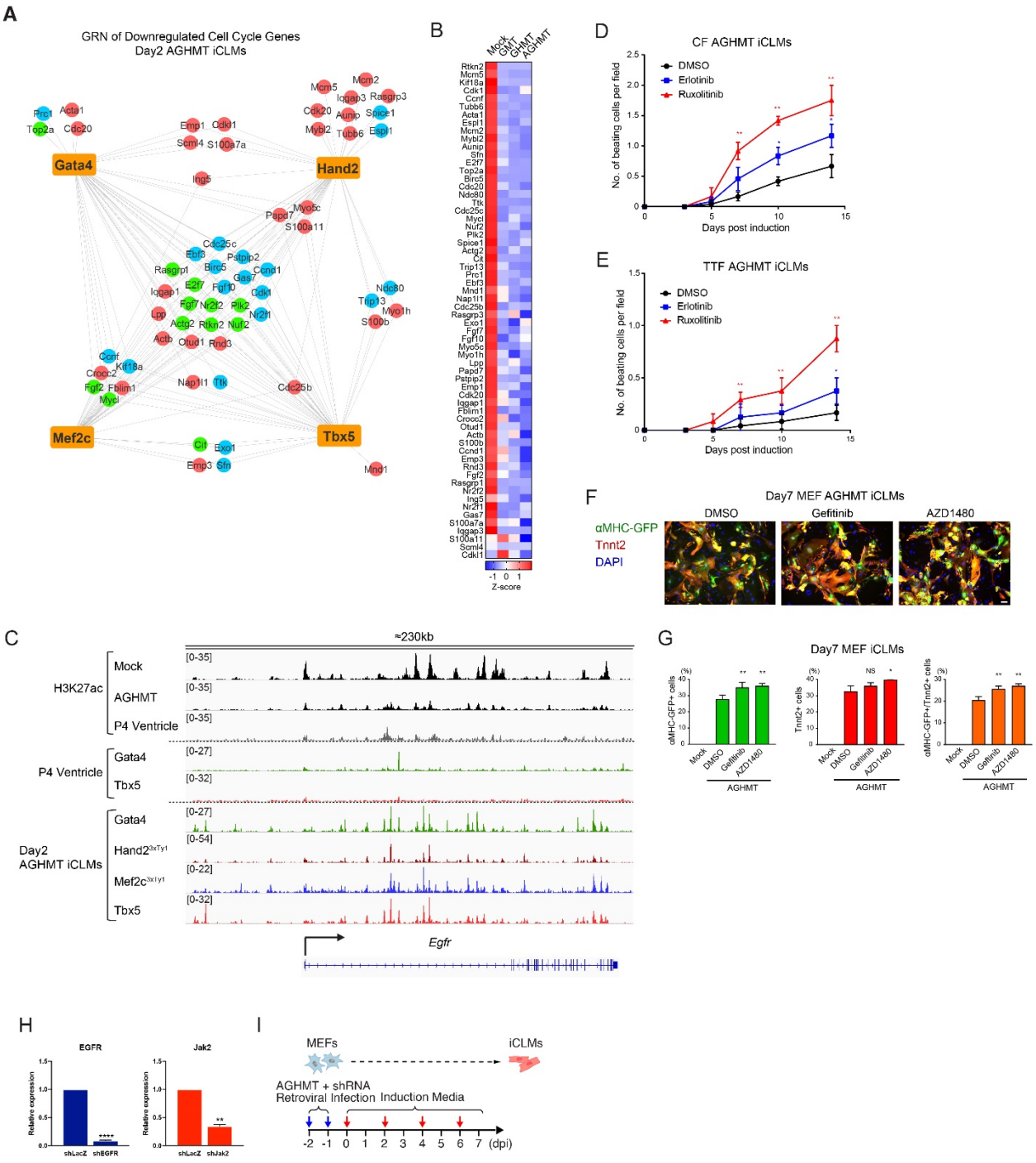
A
GRN of Downregulated Cell Cycle Genes
Day2 AGHMT iCLMs
Gata4
Hand2
Mef2c
Tbx5
B
Mock
GMT
GHMT
AGHMT
Z-score
C
≈230kb
H3K27ac
Mock
AGHMT
P4 Ventricle
P4 Ventricle
Gata4
Tbx5
Day2
AGHMT iCLMs
Hand2
Mef2c
Egfr
D
CF AGHMT iCLMs
DMSO
Erlotinib
Ruxolitinib
No. of beating cells per field
Days post induction
E
TTF AGHMT iCLMs
F
Day7 MEF AGHMT iCLMs
DMSO
Gefitinib
AZD1480
αMHC-GFP
Tnnt2
DAPI
G
Day7 MEF iCLMs
αMHC-GFP+ cells
Tnnt2+ cells
αMHC-GFP+/Tnnt2+ cells
AGHMT
H
EGFR
Jak2
Relative expression
shLacZ
shEGFR
shJak2
I
MEFs
iCLMs
AGHMT + shRNA
Retroviral Infection Induction Media
(dpi)

Figure S7, related to Figure 7. Suppression of Cell Cycle Related Genes during Reprogramming.

(A) GRN of downregulated cell cycle pathway genes in day 2 AGHMT iCLMs. Each node represents a gene and edges are drawn to all the annotated genes of reprogramming TF peaks.

(B) Gene expression heatmap of all genes from (A).

(C) A genome browser view of the *Egfr* locus showing multiple unique TF peaks and dampening of H3K27ac signal in AGHMT iCLMs.

(D,E) Quantification of spontaneous beating CF (D) and TTF (E) iCLMs after treatment (n=3, independent experiments). (* $P< 0.05$ vs. AGHMT+DMSO, ** $P< 0.01$ vs. AGHMT+DMSO). Data represented as mean ± SD.

(F) Representative immunocytochemistry images of AGHMT reprogrammed fibroblasts from αMHC-GFP transgenic mice treated with DMSO or the indicated chemicals. Cells were fixed and stained for αMHC-GFP (green), Tnnt2 (red), and DAPI (blue) 7 days after infection. (Bars, 100μm).

(G) Quantification by flow cytometry of αMHC-GFP+ and Tnnt2+ iCLMs 7 days after treatment with AGHMT and DMSO or the indicated chemicals (n=3, independent experiments). (* $P< 0.05$ vs. AGHMT+DMSO, ** $P< 0.01$ vs. AGHMT+DMSO). Data represented as mean ± SD.

(H) Suppression of *Egfr* and *Jak2* transcript levels in MEFs 2 days after infection of shRNAs (n=3, independent experiments). Transcript levels are normalized to 18S. (** $P< 0.01$ vs. shLacZ, **** $P< 0.0001$ vs. shLacZ). Data represented as mean ± SD.

(I) Strategy for knockdown by shRNA during direct cardiac reprogramming in MEFs. shRNAs were retrovirally delivered to MEFs together with the reprogramming factors. (dpi, days post induction).

Table S1, related to Figures 1 and S2. Summary of TF occupancy in day2 iCLMs.

	GMT	GHMT	AGHMT
Single	9372 (66.9%)	13660 (53.6%)	20868 (50.2%)
Two	3584 (25.6%)	6657 (26.1%)	11037 (26.5%)
Three	1054 (7.5%)	3743 (14.7%)	6791 (16.3%)
Four	-	1447 (5.7%)	2900 (7.0%)
Total	14010	25507	41596

TF Peaks with single TF occupancy

	GMT	GHMT	AGHMT
Gata4	1613 (17.2%)	1769 (13.0%)	7037 (33.7%)
Hand2	-	4531 (33.2%)	5901 (28.3%)
Mef2c	3362 (35.9%)	2506 (18.3%)	2125 (10.2%)
Tbx5	4397 (46.9%)	4854 (35.5%)	5805 (27.8%)
Total	9372	13660	20868

TF Peaks with two TF occupancy

	GMT	GHMT	AGHMT
GM	480 (13.4%)	332 (5.0%)	786 (7.1%)
GT	1663 (46.4%)	1260 (19.0%)	4471 (40.5%)
MT	1441 (40.2%)	838 (12.6%)	781 (7.1%)
GH	-	859 (12.9%)	1609 (14.6%)
HM	-	1011 (15.2%)	584 (5.3%)
HT	-	2357 (35.4%)	2806 (25.4%)
Total	3584	6657	11037

TF Peaks with three TF occupancy

	GMT	GHMT	AGHMT
GMT	1054 (100%)	383 (10.2%)	1294 (19.1%)
GHM	-	352 (9.4%)	421 (6.2%)
GHT	-	1793 (47.9%)	4401 (64.8%)
HMT	-	1215 (32.5%)	675 (9.9%)
Total	1054	3743	6791

TF Peaks with four TF occupancy

	GMT	GHMT	AGHMT
GHMT	-	1447	2900

Table S2, related to Figure 2. Known motifs recovered from reprogramming enhancers in day 2 iCLMs. Percent of target describes the frequency of motifs discovered at the target sites. Reprogramming TFs are highlighted in bold.

Symbol	Motif	GMT-Enhancer P-Value	GMT-Enhancer % of Targets	Hand2-Enhancer P-Value	Hand2-Enhancer % of Targets	Akt1-Enhancer P-Value	Akt1-Enhancer % of Targets
Nfib	NF1-halfsite(CTF)	1.00E-14	18.54	1.00E-09	20.41	1.00E-20	18.55
Meis1	Meis1(Homeobox)	1.00E-15	20.24	0.001	20.23	1.00E-17	19.31
Tgif1	Tgif1(Homeobox)	1.00E-14	36.1	1.00E-06	36.62	1.00E-17	34.45
Tgif2	Tgif2(Homeobox)	1.00E-11	37.48	1.00E-08	38.69	1.00E-14	36.33
Smad2	Smad2(MAD)	1.00E-13	17.11	1.00E-08	19.79	1.00E-14	16.4
Smad3	Smad3(MAD)	1.00E-12	32.49	1.00E-07	36.67	1.00E-08	31.42
Smad4	Smad4(MAD)	1.00E-16	17.4	1.00E-11	20.61	1.00E-13	16.74
Mef2a	Mef2a(MADS)	1.00E-122	8.22	1.00E-27	6.16	1.00E-24	4.56
Mef2b	Mef2b(MADS)	1.00E-160	14.56	1.00E-34	11.47	1.00E-36	8.94
Mef2c	**Mef2c(MADS)**	**1.00E-132**	**8.82**	**1.00E-38**	**6.8**	**1.00E-31**	**5.04**
Mef2d	Mef2d(MADS)	1.00E-104	4.69	1.00E-26	3.07	1.00E-29	2.29
Ar	AR-halfsite(NR)	1.00E-11	42	0.001	46.64	1.00E-16	42.48
Stat4	STAT4(Stat)	0.0001	10.16	1.00E-06	11.29	0.001	9.94
Tbx5	**Tbx5(T-box)**	**1.00E-16**	**34.43**	**1.00E-06**	**36.86**	**0.001**	**32.28**
Gata3	GATA3(Zf)	1.00E-65	21.27	1.00E-31	20.01	0.001	15.29
Gata1	Gata1(Zf)	1.00E-34	8.45	1.00E-20	7.95	0.001	5.75
Gata4	**Gata4(Zf)**	**1.00E-51**	**14.39**	**1.00E-25**	**13.4**	**1.00E-06**	**10.17**
Gata6	Gata6(Zf)	1.00E-56	13.43	1.00E-26	12.37	1.00E-06	9.35
Zfp711	ZNF711(Zf)	1.00E-07	14.64	0.0001	17.67	1.00E-28	16.42
Zfx	ZFX(Zf)	1.00E-08	11.86	1.00E-05	13.75	1.00E-33	13.26
Atoh1	Atoh1(bHLH)	1.00E-06	11.29	1.00E-15	14.25	1.00E-11	11.66
Hand2	**Hand2(bHLH)**	**1.00E-13**	**6.19**	**1.00E-20**	**7.58**	**1.00E-09**	**5.53**
Myod1	MyoD(bHLH)	0.0001	7.9	1.00E-07	8.67	0.001	7.94
Neurod1	NeuroD1(bHLH)	0.0001	8.36	1.00E-07	10.44	1.00E-07	8.48
Neurog2	NeuroG2(bHLH)	1.00E-07	16.52	1.00E-11	19.66	1.00E-13	16.8
Olig2	Olig2(bHLH)	1.00E-07	20.91	1.00E-07	24.51	1.00E-09	20.65
Tal1	SCL(bHLH)	1.00E-08	46.44	1.00E-05	51.33	1.00E-20	47.33
Tfap4	Ap4(bHLH)	1.00E-07	12.84	0.0001	14.49	1.00E-07	12.83
Rbpj	Rbpj1	1.00E-09	15.55	1.00E-07	16.74	1.00E-05	15.02

Table S3, related to Figure 2. Known motifs recovered from enhancers gained by day 7 compared to day 2 iCLMs. Percentage of targets describes the frequency of motifs discovered at the target sites. Reprogramming TFs are highlighted in bold.

Symbol	Motif	GMT P-Value	GMT % of Targets	GHMT P-Value	GHMT % of Targets	AGHMT P-Value	AGHMT % of Targets
Ar	AR-halfsite(NR)	1.00E-05	36.83	1.00E-05	37.7	1.00E-05	36
Bapx1	Bapx1(Homeobox)	0.1	19.66	1	19.72	1.00E-06	20.05
Nr2f2	COUP-TFII(NR)	0.01	14.11	0.01	14.54	1.00E-06	14.02
Ctcf	CTCF(Zf)	1.00E-09	1.06	0.1	0.83	0.1	0.61
Esrra	Erra(NR)	1.00E-06	18.62	1.00E-06	19.14	1.00E-06	18.13
Esrrb	Esrrb(NR)	1.00E-05	5.96	0.0001	5.89	1.00E-09	5.92
Gata1	Gata1(Zf)	1.00E-06	6.66	1.00E-05	6.19	0.01	6.03
Gata2	Gata2(Zf)	0.0001	7.45	1.00E-05	7.13	0.01	6.92
Gata4	**Gata4(Zf)**	**1.00E-07**	**11.86**	**0.001**	**10.92**	**0.001**	**11.2**
Gata6	Gata6(Zf)	1.00E-06	10.96	0.01	9.92	0.01	10.15
Mef2a	Mef2a(MADS)	1.00E-18	5.84	1.00E-29	5.69	1.00E-35	6.16
Mef2b	Mef2b(MADS)	1.00E-35	11.49	1.00E-27	10.62	1.00E-50	11.82
Mef2c	**Mef2c(MADS)**	**1.00E-35**	**6.9**	**1.00E-28**	**6.04**	**1.00E-38**	**6.73**
Mef2d	Mef2d(MADS)	1.00E-31	3.23	1.00E-20	2.88	1.00E-32	3.14
Nfib	NF1(CTF)	0.001	2.76	1.00E-06	2.96	0.1	2.4
Sox15	Sox15(HMG)	1	11.35	1	10.99	1.00E-09	12.08
Thrb	THRb(NR)	1.00E-05	36.81	1.00E-08	37.7	1.00E-09	36.58
Tlx1	Tlx(NR)	1.00E-08	3.45	0.01	3.47	1	2.77
Zfp418	ZNF416(Zf)	0.0001	10.99	0.1	10.98	1.00E-07	10.55

Table S5, related to Figures 4 and S4. List of VISTA mouse elements and Reprogramming Enhancers used to confirm *in vivo* cardiac activity by LacZ transgenic mouse assay.

Enhancer ID	Enhancer coordinates (mm10)	Enhancer length(bp)	Enhancer activation dependence	TF co-occupancy dependence	Bracketing genes
mm64	chr19:53715915-53717934	2019	GMT	GMT	Rbm20 (intragenic)
mm67	chr11:65207498-65210380	2882	GMT	GMT	Myocd (intragenic)
mm69	chr9:64044784-64046949	2165	GMT	GMT	1700055C04Rik-1110036E04Rik
mm71	chr8:95426508-95428314	1806	GMT	GMT	Gtl3 (intragenic)
mm72	chr3:152304130-152305473	1343	Mock	GMT	Fam73a (intragenic)
mm78	chr12:83072395-83074413	2018	Akt1	Hand2	Rgs6 (intragenic)
mm82	chr17:73022163-73024151	1988	GMT	GMT	Lbh-Lclat1
mm86	chr3:20145236-20146308	1072	Mock	GMT	Gyg (intragenic)
mm87	chr10:45228613-45231786	3173	Hand2	GMT	Prep-Popdc3
mm104	chr15:66824301-66827162	2861	Hand2	GMT	Sla-Tg
mm130	chr9:24887072-24890068	2996	Hand2	Hand2	Tbx20-Herpud2
mm145	chr4:120391603-120393946	2343	GMT	GMT	Foxo6-Scmh1
mm146	chr11:77422469-77424441	1972	GMT	GMT	Ssh2 (intragenic)
mm152	chr18:80330119-80332361	2242	Hand2	Hand2	Kcng2 (intragenic)
mm169	chr7:80445068-80446500	1432	Hand2	Hand2	Furin-Blm
mm174	chr7:125764047-125765353	1306	Hand2	Hand2	D430042O09Rik (intragenic)
mm245	chr14:63367789-63369845	2056	GMT	GMT	Gata4-Blk
mm1343	chr11:54879186-54884157	4971	GMT	GMT	Hint1-Gpx3
Putative Gja5	chr3:97062652-97063357	705	Hand2	Hand2	Gja5-Acp6
Putative Tnni1	chr1:135800059-135801243	1184	GMT	GMT	Tnni1 (intragenic)

Table S6, related to Figures 6 and 7. Number of genes in each cluster of day 2 AGHMT iCLMs GRN.

	Upregulated GRN	Downregulated GRN
Gata4	86	85
Hand2	91	105
Mef2c	31	32
Tbx5	76	77
GM	19	13
GT	107	85
MT	27	10
GH	52	62
HM	28	24
HT	93	64
GMT	70	42
GHM	38	22
GHT	332	265
HMT	56	28
GHMT	700	290
Total	1806	1204